

THE WATER-MEMBRANE INTERFACE PROMOTES SELF-ORGANIZATION
OF AMPHIPATHIC POLYPEPTIDE CHAINS INTO β SHEETS

Ana Nikolic,¹ Stéphanie Baud,² Sarah Rauscher^{1,3}, and Régis Pomès^{1,3,#}

¹ Molecular Structure and Function, Hospital for Sick Children, Toronto, Ontario, Canada

² Laboratoire de Biochimie, CNRS UMR 6198, IFR 53 Biomolecules, Université Champagne-Ardennes, Reims, France

³ Department of Biochemistry, University of Toronto, Toronto, Ontario, Canada

Corresponding Author. Mailing address: Molecular Structure and Function, Hospital for Sick Children, 555 University Ave., Toronto, Ontario, Canada M5G 1X8. Email: pomes @ sickkids.ca.

To be submitted to *J. Amer. Chem. Soc.*, 21 December 2007.

ABSTRACT The interaction of non-native peptides and proteins with biological membranes is implicated in numerous pathogenic processes such as including cholera, gastric ulcers, and lupus toxic wawa, and wawa wawa. In addition, recent studies suggest that the toxicity of several neurodegenerative diseases such as Alzheimer's and, etc, etcParkinson's, involves the interaction of oligomeric aggregates of amyloidogenic proteins with the neuronal membrane. We examine the physical and structural basis of peptide adsorption and aggregation in a model membrane using molecular dynamics simulations. Blocked amphipathic octameric peptides with of a simple, repetitive sequence, GVGVGVGV, are used as models of β -sheet-forming polypeptide chains found in the core of amyloid fibrils. Placed in aqueous solution in the presence of an n-octane slab mimicking the nonpolar core of lipid membranes, the peptides spontaneously partition at the octane-water interface. Adsorption displaces the conformational

equilibrium of the polypeptide chain from a heterogeneous ensemble characterized by a high degree of structural disorder towards a more ordered ensemble containing β -hairpins and elongated β -strand conformations. These conformations are favoured by the partition of the nonpolar valine side chains into the octane phase, while the methylene group of glycine points into the aqueous phase and the polypeptidic backbone lies on the water-membrane interface. Once adsorbed at the interface, peptides spontaneously aggregate and rapidly evolve β -sheet structures on a 10-ns time scale, whereas aggregates of the same polypeptide chains in water remain amorphous over considerably longer time scales. The dramatic promotion of β -sheets at the water-membrane interface results from the combination of the hydrophobic effect and of reduced conformational entropy of the polypeptide chain. While the hydrophobic effect drives interfacial partition and promotes β -strand conformations of individual polypeptide chains, the planar interface further facilitates β -sheet organization by reducing the dimensionality of the conformational search leading to self-assembly from 3D to 2D. We discuss the general relevance of these findings to the formation of amphiphilic β -sheets at the surface of globular proteins, the folding of β -barrel proteins found in the outer-membrane of gram-negative bacteria, and amyloid self-organization on the surface of biological membranes and amorphous aggregates.

Introduction

The β -sheet is one of the most common structural elements in folded proteins. Sheets are diverse, and able to form a variety of structural elements, such as β -barrels, greek key motifs, and extended sheets, so understanding the driving forces behind their formation is an important task. The determinants of β -sheet formation are made even more interesting because of the role that β -sheet structures formed by misfolded peptides play in amyloid diseases, including Alzheimer's disease ($A\beta$ and Tau), Huntington's disease (poly-glutamine), and Parkinson's disease (α -synuclein)¹.

Many different patterns of amino acid polarity are observed within β -sheets, but the most common patterns typically have a periodicity of two. Of all of these patterns, the pattern with alternating polar and non-polar residues has been found to be particularly significant². These types of patterns are generally found on β -sheets found at the interface of water and the protein's hydrophobic core. Because these regions are essentially interfaces between a polar phase (the water) and a comparatively non-polar phase (the hydrophobic core), these sorts of interfaces may play some role in helping these segments of proteins to attain the correct conformation. Another interesting aspect of alternating sequences is that they have also been shown to be capable of aggregating and forming amyloid-like fibrils³. Because of this, alternating polar-nonpolar sequences are an interesting test system, as they appear to be relevant both to β -sheets in correctly folded, non-pathological proteins, and to β -sheets as found in pathogenic aggregation with amyloid fibrils.

Amyloid fibrils are thin, elongated, insoluble structures often found in extracellular plaques around affected cells¹. Structural studies have shown that mature amyloid fibrils consist

of many copies of aligned short peptide fragments, usually between 6 and 12 residues in length, forming the characteristic structure of the amyloid fibril, known as a cross- β sheet. These structures often involve many intertwined strands of cross- β sheets^{4,5,6}. Fragments of many known amyloid disease peptides, including ones from A β and α -synuclein, have been shown to form this same structure, despite having vastly different amino acid sequences⁷. Furthermore, stretches of as few as six residues from amyloidogenic peptides have been found to induce apoptosis in cell culture⁸. In the case of calcitonin, a four residue peptide was found to have amyloid-forming activity⁹. Furthermore, recently proposed models for IAPP/amylin and α -synuclein both suggest that the amyloid forms of these peptides consist of short stretches of β -sheet connected by hairpin loops^{10,11}. All of this evidence suggests that short sequences are able to form amyloid, and that short sequences provide good models of β -sheet assembly and amyloidogenesis.

Specific properties of the cross β -sheet, such as its diameter and the number of strands wound together into the mature fibril, are dependent on the peptide sequence, although the general structural motif remains unchanged. Structural studies of fibrillization of different short peptides featuring repeats of only one amino acid (such as polylysine) have found that all these were capable of aggregating and forming fibrils, and that the sequence only affected the packing and the register of the mature fibril, while retaining the characteristic cross- β structure¹². Recent crystallization experiments with fragments of several amyloidogenic peptides showed all of them to have the same amyloid structure, except with sequence-specific differences in packing and register⁷. Because there is a vast body of evidence showing that amyloid formation is triggered by short sequences, the behaviour of these short sequences can be used as an appropriate model

for understanding the overall processes and fundamental mechanisms governing amyloid formation and toxicity.

One factor that has been found to affect the rates at which amyloid fibrils form is the presence of membranes, which are essentially a more complex case of a water-nonpolar interface. For example, the presence of sub-micellar concentrations of SDS was found to promote conversion of PrP (Prion protein) into its infectious form and increase its aggregation¹³. Several studies have found that lipids are capable of driving the formation of amyloid fibrils. In particular, liposomes with a high content of negatively charged lipids have been found to promote amyloidogenesis in proteins as diverse as insulin, G3P dehydrogenase, myoglobin, and Aβ^{14,15}. Acidic liposomes were also found to accelerate fibril formation in a fragment of the immunoglobulin light chain, as well as in the Aβ peptide^{16,15,17}.

Membranes are more than just scaffolds: studies show that the toxicity of several amyloid species, including α-synuclein, has been associated with binding and permeabilization of liposome vesicles¹⁸. Membrane binding was also found to increase the rates of α-synuclein aggregation as well as induce cell death^{19,20}. Aβ has also been found to affect membrane properties by facilitating formation of domains, rather than through direct formation of channels²¹. Fibrillization of IAPP, a protein found in diabetes, has also been shown to involve uptake of lipids, leading to cytotoxicity²². The E. coli protein HypF has also been found to interact with phospholipid bilayers and cause destabilization, especially in the presence of anionic lipids²³. In nearly all of these cases, however, mature fibrils have been found to be inert. Membranes may not always catalyze amyloid formation, as there is also some evidence that lipid binding by peptides like α-synuclein can, in certain cases, stabilize the peptide and inhibit

toxicity, suggesting that membranes do not always lead to unfolding²⁴. This suggests that the toxicity of amyloid is intimately related to membranes and to oligomers formed in the early stages of amyloidogenesis. Furthermore, it suggests that interactions with interfaces may also be related to the observed toxicity of some amyloid species.

Although the final structure of amyloid fibrils is known, the early steps of amyloid fibril formation remain unclear. These are of interest as studies have shown that the toxicity of oligomers, that is, the early intermediates of aggregation, is far greater than that of mature fibrils²⁵. Oligomer toxicity has also been shown for oligomers of fragments of amyloidogenic peptides that are only six residues in length, suggesting that amyloid toxicity results from a shared structural property, rather than from specific properties of particular peptides⁸.

Though much is known about the structure of mature amyloid fibrils, the mechanism by which they form, the factors that help in their formation, and the intermediates through which they must pass are still unclear. Models of amyloid formation are generally based on the principle of nucleation and propagation, and require the formation of a so-called “critical nucleus”¹. These models often include the concept of seeded aggregation, that is, the requirement to form an aggregate of a particular size before substantial amounts of aggregation can occur²⁶. In vitro, amyloid formation has been experimentally shown to be partly reversible, especially in its early stages, suggesting that aggregation is a reversible equilibrium reaction²⁷. Also, recent work by Xue and coworkers suggests that rearrangement of early-stage oligomers via fragmentation, that is, breakage and reforming of interactions between peptide chains, plays an important role in the kinetics of amyloid formation²⁸. There is also experimental evidence that elongation may proceed by the linear addition of monomers to the end of the elongating fibril²⁹.

Although experimental data for aggregation and amyloid formation on lipid-water interfaces are limited, existing studies of this subject suggest that interfaces amplify kinetics, although they are limited in the amount of amyloid they can form because of density-dependence and limited surface area³⁰. Understanding the ways in which interfaces modulate the formation of β -sheet could help better understanding of the *in vivo* mechanisms by which amyloid is formed, as the presence of lipid membranes and crowding within the cells could potentially have significant repercussions on the mechanism by which amyloid forms.

Small peptide fragments appear capable of forming amyloid in a relatively sequence-independent manner, and there is evidence that membranes may affect the kinetics of this process. As amyloid may have a common mechanism of formation, elucidating what is happening at the atomic level in the early stages of fibril formation would improve our understanding of the structure of early aggregates, and potentially help us to glean insight into their mechanisms of toxicity. Since early aggregates are transient and very small in size, molecular dynamics is an ideal technique for studying this aspect of amyloid formation, as MD can give us insight into what is happening at the atomic level. Because of the level of detail attainable with MD, it may also help us to understand the interactions between peptides and membranes, and help clarify the role of hydrophobic interfaces in the process of amyloidogenesis.

Molecular dynamics simulations of amyloid have revealed much information about the nature of mature fibril structure and stability, and the formation of small oligomers in water³¹. Furthermore, results from coarse-grained simulations have shown support for the nucleation-propagation mechanisms suggested by *in vitro* data³². Simulations have been performed not only

on full-length amyloidogenic peptides such as A β (1–42), but also on various short amyloid-forming peptides (e.g. ^{33,34}). Although long-scale studies have been useful for evaluating the kinetic relevance of nucleation-propagation models³⁵ and improving our understanding of fibril structure, the molecular basis of interactions between interfaces and peptides is still not well understood. Recent simulations have investigated the interactions of amyloid-forming peptides with membranes or interfaces, however, they did not examine aggregation dynamics^{36,37,38}. Our work is the first thorough investigation into the role of water-hydrophobic interfaces in the formation of β -sheets at the molecular level.

Although there are many different short fragments that we can study, we decided to focus on the sequence GV4. This sequence has a very similar motif to the sequence (GGVGV)_n, a fragment of elastin that has been experimentally shown to form fibrils³⁹. Moreover, GV4 is a similar structural motif to the sequence (GA)_n, a common component of many rigid spider silks that are also known to have an amyloid-like structure⁴⁰. Furthermore, as it consists of an alternating polar-non-polar sequence, it represents a pattern commonly found in natively β -sheet structured proteins². Previous simulations from our lab have predicted that an extended (GV)_n repeat is capable of forming amyloid⁴¹. Herein we intend to investigate the binding to an octane slab and the aggregation of the GV4 peptide. Through all-atom molecular dynamics simulations, we hope to glean more insight into the role of interfaces in intermolecular β -sheet assembly, a process that is related not only to amyloid pathology, but which may also be relevant to proper folding of β -sheets in proteins.

Methods

Simulation parameters:

All simulations were performed using GROMACS 3.3.1^{42,43}. Proteins and octane were modeled using the OPLS-AA forcefield⁴⁴ and the TIP3P⁴⁵ water model was used. The simulation was run using a leapfrog algorithm with a 2 fs integration timestep. Electrostatic interactions were calculated using PME, with a gridsize of 0.12 and updating of the neighbourlist every 10 steps⁴⁶. Lennard-Jones interactions were treated using a twin-range cut-off with a short-range and long-range cut-offs of 0.9 and 1.4 nm respectively. Pressure coupling was semi-isotropic, using the Berendsen barostat and a coupling constant of 4 ps, with a fixed Z-axis to prevent contraction of octane⁴⁷. Protein, octane and water atoms were placed in separate temperature coupling groups, and temperatures were coupled independently with a coupling constant of 0.1 ps. Constraints were treated with LINCS⁴⁸, and water was treated with the SETTLE algorithm⁴⁹. Each simulation was position restrained and equilibrated for 400 ps at constant pressure before the production runs were begun. Simulations were performed as specified in *Table 1*.

Generation of the Octane Slab

The octane slab used in Simulations B through D was generated by tiling octane atoms to form a slab at the center of the box, and then hydrating the system. The resultant system was energy-minimized and simulated for 600 ps under isotropic pressure coupling. This was enough time to allow waters that had been placed within the slab to return to the aqueous phase and for the octane slab to equilibrate.

System preparation:

All GV₄ peptides were capped with amide and acetyl groups to stabilize the peptides and

reduce the repulsive effects of terminal charges on dimer formation. The initial conformations for the peptides were taken from an ensemble generated at 296 K by simulated tempering within our laboratory. Peptides and octane were joined together and hydrated using either the GROMACS utilities (for most systems) or an in-house method (for Simulation A) to keep water out of the slab. The resultant systems were energy minimized and position restrained at NPT for 400 ps. After this, the production runs were started.

To allow peptides to accumulate on the surface while minimizing the effects of aggregation in water (e.g. in Simulation C), peptides were gradually titrated into the solution. Simulation C was generated by titrating 8, then 16, then 18 peptides onto the slab, allowing them to equilibrate until all peptides had adsorbed to the slab (which typically took about 10 ns). Measurements were started after 32 ns and 3 titrations.

The systems in Simulation D were generated by removing the octane from the simulation box and then bringing atoms from the two sides together to fill the gap formed by the removal of the octane. This way we created a system that had a smaller Z axis but was otherwise approximately equivalent to the water phase of the slab systems of Simulation B1. Although the system was designed to mimic the water phase of B1, the effective concentration was higher, since all 8 peptides could interact with each other, while the two equivalent surfaces present on the slab separated the peptides into two non-interacting groups of approximately 4 chains.

Analysis

i) Distance

Two different distance metrics were calculated for the peptides: the distance of the center of mass of the peptide from the slab on the Z axis (a measure of adsorption) and the end-to-end

distance d_{ete} , which is the three-dimensional Euclidean distance between the first and last C α atoms within the peptide, and provides a measure of extension. To determine the location of the slab, the density of octane was measured in sections along the Z-axis, normal to the slab interface, and the locations where the density crossed 650 kg/m³ were used as approximate markers for the starting and ending points of the slab.

ii) Axial distribution

In order to compensate for potential ruggedness on the octane surface, axial distributions of groups of atoms were generated by computing the distance from the octane slab surface using a Voronoi tessellation-based method similar to that of Pandit et al⁵⁰. Because octane is not ordered in the same way as a bilayer, as its atoms are uniformly distributed throughout the octane phase, the octane C atoms were put on a grid of a set size (in this case 1 nm x 1 nm). Then, the highest and lowest octane C on each point in the grid was chosen, and those atoms were used to construct the tessellation. The Z-coordinates used are those of actual atoms within the simulation, rather than guesses of the interface boundary based on center-of-mass or density, providing an improved estimate of distances from the surface of the octane compared to methods that use the center of mass of the slab phase to calculate the axial distribution of groups to the slab surface.

iii) Hydrogen Bonding

Putative hydrogen bonds were identified as any contacts where the distance between putative donor and acceptor molecules was less than 0.35 nm and that between the hydrogen and the acceptor was less than 0.25 nm. Furthermore, the angle Donor-Hydrogen-Acceptor was calculated and only accepted if it was less than 60°. In addition to these geometrical restraints,

the DSSP hydrogen bonding energy criterion was considered.⁵¹ A bond matches this criterion if its bond energy is in the range of -0.5 to -9.9 kcal/mol. If a putative hydrogen bond matched all of the above criteria, it was accepted as a hydrogen bond.

iv) Secondary Structure

The levels and types of secondary structure in the samples were predicted using the DSSP algorithm⁵¹, with adjustments to distance calculations in order to account for the presence of periodic boundary conditions.

v) Hydration Analysis

Backbone hydration & bound waters:

The hydration of the peptide backbone was analysed by calculating the number of hydrogen bonds to water for each peptide backbone group (either CO or NH). The hydrogen bonds were calculated using the same criteria outlined for backbone peptide-peptide hydrogen bonds. The raw hydrogen bonding data was then used to count the number of waters that were bound to each chain at each timepoint in the simulation. The per-chain data were used to compare backbone bound waters with other per-chain properties, such as end-to-end distance.

Side chain hydration:

Because carbon atoms cannot form hydrogen bonds to water, the hydration analysis for the side chains of GV4 consisted of measuring the number of water oxygen atoms within the cut-off for each valine C γ . A cut-off of 0.43 nm was chosen because it corresponds to the first minimum in the radial distribution function of water oxygen to the C γ atoms of valine (data not shown), encompassing the first hydration shell around the methyl group.

vi) Other analyses

Tools from the GROMACS toolkit were used to perform all other analyses and distance calculations (except d_{ete} in Simulation A, which was calculated without PBC because of the small system size). Images were generated with UCSF Chimera⁵².

Kinetics were calculated by performing a least-squares exponential fit on the proportion of peptides that were in water (that is, the initial state) at each timepoint to an equation of the form $f(x) = a \cdot e^{-bx} + c$. The coefficients obtained by the fitting were then used to solve for the equilibrium constant K by obtaining the forward and reverse reaction rates. Error was calculating using the confidence bounds for each parameter obtained by the fitting procedure.

vii) Error Analysis

Standard error of histograms was calculated using block averaging⁵³, and the error bars represent the upper and lower bounds of the 95% confidence interval of the mean.

Results

General Results

All of the simulations we performed with GV4 in the presence of the octane slab showed an irreversible binding behaviour of GV4 to the slab. Because GV4 is a disordered peptide, it was found to adopt a large number of different conformations when it bound to the slab. Some of those conformations are shown in *Figure 1*. These can be loosely separated into three categories based on the separation of the ends of the peptide, hereafter referred to as the end-to-end distance (d_{ete}). Conformations with a very narrow separation of the ends (left panel), exhibit some hairpin-like conformations, although they do not always have hydrogen bonds. Those with intermediate end-to-end separation show a diverse set of conformations, some of which show hydrogen bonding and resemble loose turns of various sorts, and others, which do not show hydrogen bonding at all. The last class of conformations (right panel) are extended, and do not have any hydrogen bonding.

After testing the binding of monomers to the slab, we decided to investigate the effects of placing several peptides on the same leaflet of the slab, and looked at aggregation over a longer timescale. Figure 14 shows some snapshots from one of the runs of Simulation B2. As the simulation progresses, hairpins and short β -structure segments consisting of either two extended peptides or an extended peptide and a hairpin become visible. Qualitatively, β -structure increases as the simulation progresses – this increase is most notable when comparing early snapshots in the simulation, such as (a) and (b) to later ones, including (c) and (d).

To look into whether this behaviour was unique to aggregation on the slab and compare it to behaviour in water we took the starting point of Simulation B1, removed the slab, and ran the

simulation without it. These runs were collectively known as Simulation D. Initial results from Simulation D (Figure 16) showed that clumping of peptides occurred very rapidly, and that in several instances, the peptides had organized into a globular aggregate of 8 chains by the end of the 20 ns of simulation time (Figure 16). While there was some β -structure observed, it seemed less prevalent, especially considering the extensive amount of aggregation that had occurred compared to the slab phase.

To look into what would happen with peptides on the slab at higher concentrations and over a long timescale, we performed several titrations of peptides onto the octane slab, allowing them enough time to adsorb onto the slab before performing the next addition. After three additions of peptides, with a total of 40 peptides on the slab, we allowed the peptides to interact on the slab. Figure 13 shows some of the extended beta sheets observed after 219 ns of simulation time. There are numerous extended β -sheets, forming higher-order structures including trimers and tetramers. From this snapshot alone, it can be seen that the GV4 peptide is capable of forming both parallel and antiparallel β -sheets. The amounts of β -sheet shown in Figure 13 and Figure 14 are much higher than that observed in Figure 15, which is the result of one of the runs of Simulation D, after it was extended for another 160 ns. Although the timescale is similar to that in Simulation C2, the amount of β -sheet that is visible in the cluster is visibly less, suggesting that the efficiency of formation of β -sheets in water at high concentrations is not particularly high.

i) GV4 binds to a model octane slab

Simulations A and B1 revealed that the GV4 peptide has a characteristic binding behaviour to the octane slab. Binding to the slab is generally initiated by interactions between

one of the valine residues and the slab (Figure 1a). Once the peptide is fully bound all four valine residues in the GV4 peptide interact with the slab (Figure 1b). Furthermore, continued interaction with the slab promotes formation of extended conformations by the peptide. Most of the peptide adsorption to the slab occurs fairly rapidly, with 99% of all chains bound by the end of Simulation B1 at 10 ns (Figure 2). Interestingly, the number of chains adsorbed to the slab follows standard first-order kinetics. Fitting the curve to a first-order kinetics equation suggests a value of K of between 324-395, suggesting that the binding to the slab is a weakly favourable process with a ΔG of about -14.55 kJ/mol (range with errors is [-14.32 to -14.81 kJ]). This suggests that even though binding is weakly favourable, possible cooperativity between the valine residues makes the process effectively irreversible due to the difficulty of four valines dissociating from the slab within a short enough period for the peptide to detach.

Figure 3a shows a sample density profile, taken from Simulation C2. The peptide chains are all distributed very close to the octane, in the interface between the octane and water. Axial distributions of the valine $C\gamma$ atoms and the $C\alpha$ atoms of the chains for Simulation C2 show that the valines are distributed asymmetrically, and that their distribution is skewed toward the slab, with fewer than expected on the other side of the $C\alpha$ atoms. In comparison to the $C\gamma$, the $C\alpha$ atoms are distributed in a fairly symmetric way, centered at 0.5 nm from the slab. Furthermore, the main chain atoms are skewed slightly away from the octane in comparison to the $C\alpha$ atoms, likely due to the relatively polar character of the peptide backbone.

ii) Slab binding dehydrates the GV4 peptides

We decided to also investigate the effects of slab binding on hydration of the backbone and the valine sidechains. A cumulative comparison of the sidechain and backbone hydration is

shown in Figure 4. Monomers on the slab (a) show complete dehydration of side chains, which suggests that dehydration of side chains is independent of aggregation, and may be a general characteristic of peptide-interface binding. In comparison, the aggregated peptides in water show some loss of backbone hydration, having similar levels of hydration to the monomers on the slab, but their side chains are not dehydrated like those of peptides on the slab. In the results for Simulation B1, there are two distinct populations, one with a high level of side chain hydration (about 5 waters around each C γ) and high backbone hydration (about 16 waters per chain), and another with low levels of side chain hydration (centered at 1) and low backbone hydration (12 waters per chain). The hydrated population corresponds to the monomers in water, and suggests that slab binding causes a decrease in the number of bound waters, as well as dehydration of valine side chains. Results for Simulation B2 are similar, with more dehydration observed due to the longer timescale. On average, the sidechains in simulation B1 and B2 appear slightly less dehydrated than those in simulation A. This is in part due to the shorter equilibration times after slab binding in B1 and B2 compared to A, and dissipates over time, as can be seen from the results of the longer simulations in C1 and C2. Peptides in Simulation C1 and C2 resemble those in Simulation B2, but are more dehydrated due to the longer simulation timescale and greater concentrations.

iii) Peptide binding to the slab alters the conformational equilibrium of GV4

We used the end-to-end distance distribution for the GV4 peptide as a representation of its conformational equilibrium. *Figure 5* shows the distributions of end-to-end distance for Simulations A through D. All simulations on the slab have a strong peak at around 0.66 nm, with the peak being most prominent for Simulation A, and decreasing in prominence for C1 and C2.

At the same time, a plateau becomes prominent for conformations of 2 nm or longer, especially in simulations C1 and C2, as well as in B2, albeit to a lesser extent. This suggests that there is a slow exchange of closed conformations into extended conformations that persists over longer timescales. In contrast, the simulations in water have few conformations of 1.3 nm or longer, and have many conformers in the mid-range, likely corresponding to hydrogen-bonded turns. The conformations in simulation D differ slightly from the monomers in water, but, unlike the simulations of aggregates on the slab, do not exhibit a plateau in the 2.0 nm and over range. The additional bumps in the conformational distribution are likely due to the comparatively smaller amount of sampling in Simulation D in comparison to the other experiments.

To examine the evolution of the distance distribution over time we binned the end-to-end distances over periods of 500 ps. The results of this analysis for Simulations B1 and B2, shown in *Figure 6*, reveal that the extension is a rapid process, and the bulk of the extension occurs within the first 10 ns, by transitioning of conformers from the intermediate range into extended conformers. Although conversion from hairpins to extended forms can also occur, this is most likely to occur in two stages, and may involve initial conversion of the hairpin form into an intermediate form. The conversion of the hairpin into more extended conformations likely takes longer, which is why it is difficult to see at short timescales like those explored in B1 and B2.

To investigate the possibility of conformational exchange more thoroughly, we quantified the proportions of conformers in the closed/hairpin, intermediate, and extended conformations for all simulations (Figure 7). For simulations on the slab, the proportion of peptides in the closed/hairpin conformation decreases as the concentration and time spent on the slab increases, and it is most prominent in simulation C2. In contrast, the simulations in water maintain a level

of the closed conformation similar to that of the monomers on the slab, regardless of their aggregation state. Another important distinction between the slab and the water systems can be seen in *Figure 7b*, as the monomers on the slab show distinctly more extended conformations than peptides in water, regardless of their aggregation state. This effect increases along with time and concentration, and is highest in Simulation C2. This all suggests that conversion of intermediate forms into extended forms is a characteristic of GV4 binding to the slab that is observed in neither monomers nor aggregates in water. Furthermore, the frequency of hairpin conformations decreases over time, suggesting that an conversion of hairpins into more extended conformations is indeed occurring as aggregation proceeds. It is also interesting to note that there is no significant difference in the proportion of hairpin-like conformations observed in aggregates in water as compared to monomers in water and monomers on the slab.

iv) Time-evolution of hydrogen bonding

In addition to affecting the conformational equilibrium of the peptides, binding to the slab also affects the way that they form hydrogen bonds. In simulation B1 and B2, there is a linear increase in the number of hydrogen bonds formed by the peptides, resulting in almost 1.5 intermolecular hydrogen bonds formed by each chain by the end of the 30 ns. In contrast, the number of intramolecular hydrogen bonds stays firm at about 0.6 bonds per chain, suggesting that slab binding has little overall effect on the quantity of intramolecular hydrogen bonds in the ensemble. Simulation C2 (Figure 8b) represents a longer-scale and higher-concentration system, and exhibits a far higher level of hydrogen bonding, with up to 8 hydrogen bonds per chain by the end of the 219 ns simulation. Even after 219 ns, more hydrogen bonds still appear to be forming, at a relatively constant rate. Furthermore, the number of intramolecular hydrogen bonds

per chain seems to dip slightly over time, suggesting that as the peptides form ordered aggregates, the level of intramolecular hydrogen bonding gradually drops from its original state. Aggregation in water (Figure 8c) occurs with a more rapid formation of hydrogen bonds than observed for Simulation B1 and B2. One possible reason for this discrepancy is the fact that slab binding effectively dilutes the peptides, by distributing approximately four peptides on each slab surface. Another possibility is that at the concentrations in water that were tested, there are numerous possible geometries through which peptides can interact and form hydrogen bonds, many of which may become less favourable once the peptides are bound to the slab surface. The initial aggregation stage in water tapers off after about 15 ns, after which hydrogen bonds rise at a much lower rate, potentially due to rearrangements within existing aggregates rather than formation of new ones.

We also investigated whether certain conformations were more likely to participate in particular hydrogen-bonding interactions than others. To this end, we separated the end-to-end distance distribution into four mutually exclusive categories: peptides with only intermolecular hydrogen bonds, those with only intramolecular hydrogen bonds, those participating in both types of hydrogen bonds, and those with no hydrogen bonding at all. The results of this analysis show that the four classes of conformations tend to form two clusters. The peptides with either no hydrogen bonding or only intermolecular hydrogen bonds tend to be distributed in the more extended portion of the end-to-end distance range and show similar distributions. However, the peptides with only intermolecular bonds form a pronounced plateau at conformations > 2 nm, which is especially noticeable in the results from Simulation C2. In contrast, the peptides with either both types of hydrogen bonds or only intramolecular bonds exhibit very similar

distributions, likely due to the significant contribution of hairpin-like conformations to these two populations. Another notable distinction is that the divergence between the two distributions appears the greatest in Simulation C2, with several peaks appearing in the distribution for peptides with both types of hydrogen bonds, suggesting that the states with multiple types of hydrogen bonds may act as intermediates.

v) *Aggregation occurs while on the slab*

Because of the large number of intermolecular hydrogen bonds formed, we decided to examine the rate at which peptides were aggregating. To do this we counted the number of peptides that had intermolecular hydrogen bonds, and then calculated these as the fraction aggregated. In Simulation B1 and B2, about 50% of all peptides had aggregated by the end of Simulation B1, and aggregation continued at a slower rate once all peptides were on the slab (Figure 10a). After a longer period of time on the slab, as in Simulation C2, the fraction of peptides aggregated was close to 100%, that is, all peptides were participating in intermolecular bonds.

To further investigate the nature of hydrogen bonding and examine the hydration of the aggregates, we compared the backbone hydration of the peptides to the number of hydrogen bonds they formed, using the same criteria as in Figure 9. There is an anticorrelation between the number of hydrogen bonds formed and the number of backbone bound waters, suggesting that the bound waters are being replaced by hydrogen bonds formed within the aggregate. The number of hydrogen bonds increases as the timescale and concentration of the peptides increases – note the gradual increase in the maximum from simulation B1, to simulation C2. Another interesting trend occurs in the peptides with both intramolecular and intermolecular hydrogen

bonds. The relative frequency of peptides that fall into this category seems to increase from simulation B1, to B2, and onwards to C1. However, it drops off in simulation C2, even though the peptides in this category do show the largest number of hydrogen bonds in this particular simulation. This suggests that the peptides with both types of hydrogen bonds are acting as an intermediate. Their frequency increases early on in the aggregation process, and decreases gradually as aggregates mature and intramolecular hydrogen bonds are dissociated. The overall trend when these two types of peptides are combined is a gradual increase in the number and distribution of hydrogen bonds, with most chains having between 4 and 12 hydrogen bonds in simulation C2, as compared to 0 to 4 hydrogen bonds in simulation B1. A similar analysis performed for simulation D shows results similar to those for simulation B, except with the base (0 hydrogen bonds) occurring at a higher number of bound waters, suggesting that the mechanism occurring is similar, but it is occurring from a different baseline level of dehydration (data not shown).

v) *Structure of aggregates*

The large number of intermolecular hydrogen bonds seen in simulation B1, and even more so C1 and C2 suggested that the aggregates may have converted into a more ordered form. To investigate the ordering of the aggregates, we examined the secondary structure of the systems. We found that there was a notable increase in the amount of extended β -sheet structure that was formed both in Simulations B1 and B2, as well as in C1 and C2 (Figure 13). In simulations B1 and B2, the levels of β -sheet increased from none initially to 4% of all residues, and up to 6% after the end of simulation B2. The levels of β -structure observed in Simulation C1 and C2 were even more striking, with the levels of β -sheet going from 10% at the 32 ns

mark all the way up to almost 30% of all residues after 219 ns of simulation. Notably, the levels of β -bridges remained low, at around 5% of all residues, in all simulations. Because extended β -sheets are essentially β -bridges with more than two involved residues, the constant levels of β -bridges suggest that these structures may act as potential substrates for further formation of extended β -sheets. These were the main contributors to hydrogen-bonded structure in these peptides, as the total contribution of all other hydrogen-bonded structural types (e.g. turns, helices) in Simulation B2, C1 and C2 was less than 5%.

Discussion

Implications of Slab Binding

Binding of the GV4 peptide to the slab is an interesting result, and one with the clear driving forces behind this are easy to determine forces. For example, hydrophobic interactions between the alkyl groups in the side chains of amino acids like valine and the methyl groups in octane are likely to drive association of the side chains and the octane clump. Although we can look at octane as a model of what happens at a lipid-water interface, examining the specific case of binding of peptides to clumps of saturated hydrocarbons in water also has merit. A recent study by Lee et al treated α -synuclein with hexane granules, and found that this led to rapid formation of amyloid fibrils⁵⁴. The present study suggests a theoretical explanation for the effects observed in results of these experiments, as the hexane may act as a scaffold and induce some conformational change in the α -synuclein, just as the octane slab does for the GV4 peptide. Although the effects of binding to a water-nonpolar interface likely depend on the character of the side chains involved, we believe that it is likely that such binding may induce local conformational changes in certain portions of the peptide, priming them for the formation of β - sheets.

Furthermore, the binding of peptides to an interface such as the slab acts to simultaneously dilute and concentrate them. For example, in Simulation B2, we have about 4 peptides on each side rather than 8 in one block of water – effectively diluting the concentration of peptide by 2. Yet, as peptides are titrated onto the surface, and due to the decreased number of degrees of freedom available to the peptide while it is on the surface, the local concentration of peptide increases. So in this manner, binding to an interface performs two roles. At first, it

dilutes the peptide in solution by taking peptides away from the water phase. As peptides are titrated into the solution, however, the concentration increases, and a very high local concentration of peptide can be reached in this way. Because of these concentration effects alone, the binding to the slab may act to promote the formation of β -sheets by increasing the local concentration of peptide.

The Slab as a Model

Although the slab directly models the effects of binding of hydrophobic side chains to alkanes it is also of value as a model. There are two main types of biologically relevant polar-nonpolar interfaces: the lipid bilayer, and the surface of a molten globule. Lipid bilayers differ from the slab in that they have polar and charged headgroups, and have low density and relatively high fluidity in the middle. Two major components of the bilayer structure would act to reduce the binding affinity and the kinetics of the process in comparison to that occurring on the slab. Firstly, there would be the potential for charge repulsion between polar or charged groups on the peptide backbone or sidechains and the charged or polar atoms and groups on the polar portion of the phospholipids. Furthermore, the ruggedness of the phospholipid bilayer would decrease the kinetics of peptide aggregation once they are on the slab, because diffusion would be hindered by the surface structure.

→ charge repulsion = bad = decreases activity

→ rugged surface = bad = decreases kinetics

Another biologically relevant situation that the slab may help to model is that of a molten globule. Globular oligomers of peptides have been found in many amyloid-forming peptides, and in some instances have been thought to be a precursor to the mature fibril stage, although that is

debatable. Because it is hydrophobic, behaviour on the slab may represent the behaviour of peptides at the surface of large proteinaceous aggregates. Furthermore, many models of protein folding consider hydrophobic collapse an important early step in the process. Once a protein has collapsed into a molten globule, then its exterior will in fact be in an environment rather similar to a polar-nonpolar interface, as the inside will be free of water. Furthermore, as many β -sheets, in particular antiparallel ones, in functional protein are formed near or at the water-nonpolar surface, this would provide another possible rationale for the ability of a water-nonpolar interface to drive their formation.

Relevance of GV4 peptide Kinetics of GV4

The process of nucleation and propagation commonly assumed to be the in vitro mechanism of amyloid formation may occur differently when the monomers are at least partly adsorbed to a hydrophobic interface. There are two main additional entropic considerations that come into play when dealing with interfaces that act to increase rates of ordered β -sheet formation: loss of conformational space in the chain leading to increased prevalence of extended conformations, and the replacement of 3D diffusion processes with a 2D diffusion process on the interface.

As monomers on the interface, the GV4 peptides initially tend to adopt one of two main classes of conformations, a hairpin-like conformation, which makes up approximately 30% of monomers on the slab, or one of many extended conformations, contributing about 45% in the case of monomers, and up to 70% in simulation C2. The conformational equilibrium, end-to-end distance distributions, and the prevalence of various β -hairpin like structures are similar to the results obtained by Soto et al in simulations of a 10-residue polyalanine peptide in pure

cyclohexane⁵⁵. This might suggest that exposure of peptide residues to a hydrophobic surface without complete immersion may be enough to trigger conformational changes which increase the prevalence of β -sheet and β -strand like states. This line of reasoning is also supported by the ability of sub-micellar concentrations of SDS, where the hydrophobic tails of SDS are exposed to water, to trigger preferential formation of b-structure in peptide chains.

The ratio of the two appears to depend on concentration, as when the slab is more densely populated, forming many hydrogen bonds to neighbouring extended peptides is more favourable than forming an internal hairpin. Along with the trend of increasing extended conformations with time and concentration, these data suggest that the slab indeed does lead to a large increase in levels of extended conformations, which could contribute to β -sheet formation. Binding to the slab appears to decrease the conformational freedom of the peptide, and alters its conformational equilibrium towards a greater preference of extended states.

Such extended forms can directly form ordered dimers by joining together, but our results suggest that the hairpin-like structures are capable of forming both intramolecular and intermolecular peptide-peptide hydrogen bonds simultaneously. Peptides exhibiting this class of bonding are surprisingly common, consisting of 18.9% of all peptides in Simulation C2. All of these processes are effectively equilibria, as hydrogen bonds are not permanent and interactions held together by only a few hydrogen bonds do not always last—the levels of fluctuation in the secondary structure and aggregate size metrics for GV4 support this view. Nevertheless, dimers do elongate, and eventually can form elongated sheet-like structures, like those that were observed in Simulation C2. It is important to note that despite the increase in the number of β -

sheets observed, the majority of the peptide chains are still disordered (~60-70% in Simulation C2, and higher in the other systems). The prevalence of such disordered states implies that we are still observing an early phase in amyloid formation, and that it would take far more time for the peptides in these systems to reach a fully ordered state.

Diffusion along the slab as opposed to in water also contributes to the catalysis of β -sheets. When they are adsorbed to an interface, such as the slab, peptides can remain monomers and be guided to each other through 2D diffusion. This has several benefits: it reduces the range of motion of the monomers, and discourages formation of amorphous aggregates, like those observed in Simulation D. Alignment also increases the local concentration of the peptide, as the same number of units is aligned on a two-dimensional plane rather than a three-dimensional volume, reducing their entropy and increasing the likelihood of collision. In effect, the octane slab acts as a giant scaffold, and behaves as if it was the surface of a large amorphous aggregate, only unable to hydrogen bond. Because of this, the behaviour of peptides at the surface of the octane may be similar to their behaviour at the surface of large, amorphous, hydrophobic aggregates. The only appreciable difference would be that the octane surface is flatter and more uniformly hydrophobic, making it a better scaffold of β -sheet formation. Interestingly, in systems where concentration is higher than the maximum amount of peptide that can fit on that region of the slab, there are more amorphous aggregates and less ordered dimer formation. This may suggest that density on the slab (or concentration in solvent) determines the preferred path to formation of extended β -sheets.

| Kinetically, there appears to be two distinct phases in the process that occurs when peptides are bound to the slab. There is an initial burst of activity as peptides form initial contacts

and bind to the slab, and a second, slower phase as those peptides rearrange. There are several possible ways the observed kinetics could be related to existing nucleation-propagation models. First, the very short burst of activity that occurs upon binding could be a phase unique to the slab, and the initial rearrangements that occur after it (the slow phase) could essentially be the lag phase. As the systems observed are highly disordered, it is possible that the slow growth could be representative of the lag phase. Another possibility is that the presence of the slab obviates the need for a lag phase entirely, and allows gradual linear growth to occur after peptides are bound. In both cases, it is worthwhile to note that the concentrations of peptides in our systems are orders of magnitude greater than those used for in vitro kinetics measurements, and as such, the high concentration may affect the ordering and aggregation mechanism.

LIMITATIONS OF SYSTEM

Octane (b/c is uncharged, symmetrical, way it is packed in the layer, the fact it has no curvature, etc.)

GV4 (amphipathic, very low intrinsic alpha helix propensity, no charged/polar residues)

Timescales (high concentrations are far greater than you would probably find in vivo)

Brief outline for discussion:

→ what about effects of membrane recycling and vesicular transport on all of this?

→ possible theories of slab binding

→ burial of hydrophobic residues

→ more complex sequences would have slower kinetics (predicted) but fewer

off-pathway forms because of the bulkiness of side chains and decreased number of possible stable aggregated arrangements

→ this would support why the sub-micellar concentrations of SDS etc. would cause changes rather than micellar, because of the exposure of the hydrophobic portions of the surface

→ “like likes like”

→ emphasis on DISORDERED nature of peptide in these instances (that is, a majority of the peptides are in a “coil” conformation in all cases, even when there is additional b-structure)

→ possible mechanics of aggregation on the slab

→ diffusion

→ joining of hairpins + extended → 3 extended (does that even occur?)

→ relate to known papers/theories of hairpin folding and sheet folding and important role of hairpins in folding and so on and so forth → significance of hairpins (putative intermediates)

How do our results relate to two different regimes: (a) the low concentration limit, where addition of monomer to preformed fibril is the RLS; (b) the high concentration limit, where reorganization of aggregates is the rate-limiting step (see the recent Vendruscolo papers in which they used their “tube” model)?

Discuss limitations of our molecular model.

→ comparison to known experimental/theoretical work

Conclusion

This is the first thorough investigation into the effects of binding to a water-hydrophobic interface on aggregation of short amyloidogenic peptide fragments. We have successfully characterized the structural equilibrium and the aggregation behaviour of the short peptide GV4 in solution as well as the membrane-mimetic environment of an octane slab. Our results reveal that the kinetics of aggregation on the slab, at least at the short timescales, differs significantly from the expectations set out by the nucleation-propagation model. Aggregation of GV4 on the slab and β -sheet formation appears to proceed in a linear fashion, which strengthens the possibility that lipid-rich areas of the cell such as lipid rafts may play a significant role in the assembly of β -sheets in vivo.

Binding to the slab causes significant changes in the conformational equilibrium of the GV4 peptide. Our results show that residues located at interfaces exhibit partial dehydration and a tendency to form extended conformations. Furthermore, the aggregates form large numbers of hydrogen bonds and significant levels of β -structure, particularly extended β -sheets. These tendencies suggest that exposure to hydrophobic interfaces have the potential to alter the conformational equilibrium of amyloidogenic peptides into a form more conducive to formation of extended cross- β -sheets. Although the changes induced by binding may be important in the pathology of amyloid disease, it may also be relevant to protein folding in general, as many anti-parallel β -sheets form at the interfacial regions of proteins, at the interface of the compacted hydrophobic globule in the middle and the solvent-accessible outer portion.

Also, intermolecular hydrogen bonding appears to be a way for the peptide to stabilize itself in absence of hydrogen bonds to water, driving further dehydration of the peptide chains. This effect is observable at all concentrations, but appears more pronounced at higher concentrations of GV4. In the case of GV4, at least, the presence of the interface appears to have an ordering effect, promoting the extended form of the peptide and the formation of extended β -sheet conformations.

Using the techniques developed in this study, we can investigate any number of peptides and thoroughly characterize their behaviour and aggregation at lipid-water interfaces. We can look beyond simple neutral interfaces such as octane, to more complex systems involving more biologically relevant lipids or lipid mixtures, perhaps including gangliosides and other components commonly found in lipid rafts. With recent advances in computational technology, MD remains a viable tool for studying the interactions between amyloid forming peptides and membrane-like environments, and may help us to get a clearer picture for how membranes fit into the amyloid equation.

Acknowledgments

Thanks to the Centre for Computational Biology at the Hospital for Sick Children and to SHARCNET for their very generous provision of computational resources.

1. Chiti, F. & Dobson, C.M. Protein misfolding, functional amyloid, and human disease. *Annu. Rev. Biochem* **75**, 333–366(2006).
2. Mandel-Gutfreund, Y. & Gregoret, L.M. On the Significance of Alternating Patterns of Polar and Non-polar Residues in Beta-strands. *Journal of Molecular Biology* **323**, 453-461(2002).
3. Broome, B.M. & Hecht, M.H. Nature disfavors sequences of alternating polar and non-polar amino acids: implications for amyloidogenesis. *Journal of Molecular Biology* **296**, 961-968(2000).
4. Jiménez, J.L. et al. Cryo-electron microscopy structure of an SH3 amyloid fibril and model of the molecular packing. *The EMBO Journal* **18**, 815—821(1999).
5. Serpell, L.C., Blake, C.C. & Fraser, P.E. Molecular structure of a fibrillar Alzheimer's A\$\\beta\$ fragment. *Biochemistry* **39**, 13269—13275(2000).
6. Nelson, R. et al. Structure of the cross-beta spine of amyloid-like fibrils. *Nature* **435**, 773—778(2005).
7. Sawaya, M.R. et al. Atomic structures of amyloid cross-beta spines reveal varied steric zippers. *Nature* **447**, 453—457(2007).
8. Pastor, M.T. et al. Amyloid toxicity is independent of polypeptide sequence, length and chirality. *J Mol Biol* **375**, 695—707(2008).
9. Reches, M., Porat, Y. & Gazit, E. Amyloid Fibril Formation by Pentapeptide and Tetrapeptide Fragments of Human Calcitonin. *Journal of Biological Chemistry* **277**, 35475—35480(2002).
10. Wiltzius, J.J.W. et al. Atomic structure of the cross-{beta} spine of Islet Amyloid Polypeptide (Amylin). *Protein Science* (2008).
11. Vilar, M. et al. The fold of {alpha}-synuclein fibrils. *Proceedings of the National Academy of Sciences* **105**, 8637(2008).
12. Fandrich, M. The behaviour of polyamino acids reveals an inverse side chain effect in amyloid structure formation. *The EMBO Journal* **21**, 5682—5690(2002).
13. Stohr, J. et al. Mechanisms of prion protein assembly into amyloid. *Proceedings of the National Academy of Sciences of the United States of America* **105**, 2409-14(2008).
14. Zhao, H., Tuominen, E.K. & Kinnunen, P.K. Formation of amyloid fibers triggered by phosphatidylserine-containing membranes. *Biochemistry* **43**, 10302—10307(2004).
15. McLaurin, J.A. & Chakrabarty, A. Membrane Disruption by Alzheimer beta-Amyloid Peptides Mediated through Specific Binding to Either Phospholipids or Gangliosides. *Journal of Biological Chemistry* **280**, 30001—30008(1996).
16. Zhu, M. et al. Surface-catalyzed Amyloid Fibril Formation. *Journal of Biological Chemistry* **277**, 50914—50922(2002).
17. Yip, C.M., Darabie, A.A. & McLaurin, J.A. A\$\\beta\$42-Peptide Assembly on Lipid Bilayers. *Journal of Molecular Biology* **318**, 97—107(2002).
18. Volles, M.J. et al. Vesicle permeabilization by protofibrillar \$\\alpha\$-synuclein: implications for the pathogenesis and treatment of Parkinson's disease. *Biochemistry* **40**, 7812—7819(2001).
19. Lee, H.J., Choi, C. & Lee, S.J. Membrane-bound \$\\alpha\$-Synuclein Has a High

- Aggregation Propensity and the Ability to Seed the Aggregation of the Cytosolic Form.
Journal of Biological Chemistry **277**, 671—678(2002).
20. Jo, E. et al. α -Synuclein Membrane Interactions and Lipid Specificity. *Journal of Biological Chemistry* **275**, 34328—34334(2000).
21. Valincius, G. et al. Soluble amyloid {beta} oligomers affect dielectric membrane properties by bilayer insertion and domain formation: Implications for cell toxicity. *Biophysical Journal* (2008).
22. Sparr, E. et al. Islet amyloid polypeptide-induced membrane leakage involves uptake of lipids by forming amyloid fibers. *FEBS Letters* **577**, 117—120(2004).
23. Canale, C. et al. Natively Folded HypF-N and Its Early Amyloid Aggregates Interact with Phospholipid Monolayers and Destabilize Supported Phospholipid Bilayers. *Biophysical Journal* **91**, 4575(2006).
24. Zhu, M. & Fink, A.L. Lipid Binding Inhibits α -Synuclein Fibril Formation. *Journal of Biological Chemistry* **278**, 16873—16877(2003).
25. Hartley, D.M. et al. Protomeric Intermediates of Amyloid beta-Protein Induce Acute Electrophysiological Changes and Progressive Neurotoxicity in Cortical Neurons. *Journal of Neuroscience* **19**, 8876(1999).
26. Come, J.H., Fraser, P.E. & Lansbury Jr, P.T. A Kinetic Model for Amyloid Formation in the Prion Diseases: Importance of Seeding. *Proceedings of the National Academy of Sciences of the United States of America* **90**, 5959—5963(1993).
27. Cannon, M.J. et al. Kinetic analysis of beta-amyloid fibril elongation. *Analytical Biochemistry* **328**, 67—75(2004).
28. Xue, W., Homans, S.W. & Radford, S.E. Systematic analysis of nucleation-dependent polymerization reveals new insights into the mechanism of amyloid self-assembly. *Proceedings of the National Academy of Sciences* **105**, 8926-8931(2008).
29. Collins, S.R. et al. Mechanism of prion propagation: amyloid growth occurs by monomer addition. *PLoS Biol* **2**, e321(2004).
30. Sharp, J.S., Forrest, J.A. & Jones, R.A.L. Surface denaturation and amyloid fibril formation of insulin at model lipid-water interfaces. *Biochemistry* **41**, 15810—15819(2002).
31. Urbanc, B. et al. Molecular Dynamics Simulation of Amyloid β Dimer Formation. *Biophysical Journal* **87**, 2310—2321(2004).
32. Auer, S., Dobson, C.M. & Vendruscolo, M. Characterization of the nucleation barriers for protein aggregation and amyloid formation. *HFSP Journal* **1**, 137-146(2007).
33. Wu, C., Lei, H. & Duan, Y. The Role of Phe in the Formation of Well-Ordered Oligomers of Amyloidogenic Hexapeptide (NFGAIL) Observed in Molecular Dynamics Simulations with Explicit Solvent. *Biophysical Journal* **88**, 2897—2906(2005).
34. Gsponer, J., Haberthur, U. & Caflisch, A. The role of side-chain interactions in the early steps of aggregation: Molecular dynamics simulations of an amyloid-forming peptide from the yeast prion Sup35. *Proceedings of the National Academy of Sciences* **100**, 5154(2003).
35. Nguyen, H.D. & Hall, C.K. Molecular dynamics simulations of spontaneous fibril formation by random-coil peptides. *Proc Natl Acad Sci USA* **101**, 16180—16185(2004).
36. Jang, H., Zheng, J. & Nussinov, R. Models of β -Amyloid Ion Channels in the Membrane Suggest That Channel Formation in the Bilayer Is a Dynamic Process.

- Biophysical Journal* **93**, 1938(2007).
37. Crowet, J.M. et al. In Silico tilted properties of the 67-78 fragment of \$\alpha\$-synuclein are responsible for membrane destabilization and neurotoxicity. *Proteins* **68**, 936—947(2007).
 38. Knecht, V. beta-Hairpin Folding by a Model Amyloid Peptide in Solution and at an Interface. *The Journal of Physical Chemistry. B* (2008).doi:10.1021/jp8026513
 39. Miao, M. et al. Sequence and Structure Determinants for the Self-aggregation of Recombinant Polypeptides Modeled after Human Elastin*. *Journal of Biological Chemistry* **278**, 48553—48562(2003).
 40. Kenney, J.M. et al. Amyloidogenic nature of spider silk. *FEBS Journal* **269**, 4159—4163(2002).
 41. Rauscher, S. et al. Proline and glycine control protein self-organization into elastomeric or amyloid fibrils. *Structure* **14**, 1667—1676(2006).
 42. Lindahl, E., Hess, B. & van der Spoel, D. GROMACS 3.0: a package for molecular simulation and trajectory analysis. *Journal of Molecular Modeling* **7**, 306—317(2001).
 43. Berendsen, H.J.C., van der Spoel, D. & van Drunen, R. GROMACS: A message-passing parallel molecular dynamics implementation. *Computer Physics Communications* **91**, 43—56(1995).
 44. Jorgensen, W.L., Maxwell, D.S. & Tiradore, J. Development and Testing of the OPLS All-Atom Force-Field on Conformational Energetics and Properties of Organic Liquids. *Journal of the American Chemical Society* **118**, 11225—11236(1996).
 45. Jorgensen, W.L. et al. Comparison of simple potential functions for simulating liquid water. *The Journal of Chemical Physics* **79**, 926(1983).
 46. Essmann, U. & others A smooth particle mesh Ewald method. *The Journal of Chemical Physics* **103**, 8577(1995).
 47. Berendsen, H.J.C. et al. Molecular dynamics with coupling to an external bath. *The Journal of Chemical Physics* **81**, 3684(1984).
 48. Hess, B. et al. LINCS: A linear constraint solver for molecular simulations. *Journal of Computational Chemistry* **18**, 1463—1472(1997).
 49. Miyamoto, S. & Kollman, P.A. Settle: An analytical version of the SHAKE and RATTLE algorithm for rigid water models. *Journal of Computational Chemistry* **13**, 952-962(1992).
 50. Pandit, S.A., Bostick, D. & Berkowitz, M.L. An algorithm to describe molecular scale rugged surfaces and its application to the study of a water/lipid bilayer interface. *The Journal of Chemical Physics* **119**, 2199(2003).
 51. Kabsch, W. & Sander, C. Dictionary of protein secondary structure: pattern recognition of hydrogen-bonded and geometrical features. *Biopolymers* **22**, 2577—2637(1983).
 52. Pettersen, E.F. et al. UCSF Chimera—A visualization system for exploratory research and analysis. *Journal of Computational Chemistry* **25**, 1605-1612(2004).
 53. Allen, M.P. & Tildesley, D.J. *Computer Simulation of Liquids.* (Clarendon Press: 1987).
 54. Lee, J. et al. Instantaneous Amyloid Fibril Formation of \${\alpha}\$-Synuclein from the Oligomeric Granular Structures in the Presence of Hexane. *Biophysical Journal* (2008).
 55. Soto, P., Baumketner, A. & Shea, J. Aggregation of polyalanine in a hydrophobic environment. *J Chem Phys* **124**, 134904(2006).1. Chiti, F. & Dobson, C.M. Protein misfolding, functional amyloid, and human disease. *Annu. Rev. Biochem* **75**,

- 333–366(2006).
2. Mandel-Gutfreund, Y. & Gregoret, L.M. On the Significance of Alternating Patterns of Polar and Non-polar Residues in Beta-strands. *Journal of Molecular Biology* 323, 453–461(2002).
 3. Broome, B.M. & Hecht, M.H. Nature disfavors sequences of alternating polar and non-polar amino acids: implications for amyloidogenesis. *Journal of Molecular Biology* 296, 961–968(2000).
 4. Jiménez, J.L. et al. Cryo-electron microscopy structure of an SH3 amyloid fibril and model of the molecular packing. *The EMBO Journal* 18, 815–821(1999).
 5. Serpell, L.C., Blake, C.C. & Fraser, P.E. Molecular structure of a fibrillar Alzheimer's A β fragment. *Biochemistry* 39, 13269–13275(2000).
 6. Nelson, R. et al. Structure of the cross-beta spine of amyloid-like fibrils. *Nature* 435, 773–778(2005).
 7. Sawaya, M.R. et al. Atomic structures of amyloid cross-beta spines reveal varied steric zippers. *Nature* 447, 453–457(2007).
 8. Pastor, M.T. et al. Amyloid toxicity is independent of polypeptide sequence, length and chirality. *J Mol Biol* 375, 695–707(2008).
 9. Reches, M., Porat, Y. & Gazit, E. Amyloid Fibril Formation by Pentapeptide and Tetrapeptide Fragments of Human Calcitonin. *Journal of Biological Chemistry* 277, 35475–35480(2002).
 10. Wiltzius, J.J.W. et al. Atomic structure of the cross-(beta) spine of Islet Amyloid Polypeptide (Amylin). *Protein Science* (2008).
 11. Vilar, M. et al. The fold of (alpha)-synuclein fibrils. *Proceedings of the National Academy of Sciences* 105, 8637(2008).
 12. Fandrich, M. The behaviour of polyamino acids reveals an inverse side chain effect in amyloid structure formation. *The EMBO Journal* 21, 5682–5690(2002).
 13. Stohr, J. et al. Mechanisms of prion protein assembly into amyloid. *Proceedings of the National Academy of Sciences of the United States of America* 105, 2409–14(2008).
 14. Zhao, H., Tuominen, E.K. & Kinnunen, P.K. Formation of amyloid fibers triggered by phosphatidylserine-containing membranes. *Biochemistry* 43, 10302–10307(2004).
 15. McLaurin, J.A. & Chakrabarty, A. Membrane Disruption by Alzheimer beta-Amyloid Peptides Mediated through Specific Binding to Either Phospholipids or Gangliosides. *Journal of Biological Chemistry* 280, 30001–30008(1996).
 16. Zhu, M. et al. Surface-catalyzed Amyloid Fibril Formation. *Journal of Biological Chemistry* 277, 50914–50922(2002).
 17. Yip, C.M., Darabie, A.A. & McLaurin, J.A. A β 42-Peptide Assembly on Lipid Bilayers. *Journal of Molecular Biology* 318, 97–107(2002).
 18. Volles, M.J. et al. Vesicle permeabilization by protofibrillar A β -synuclein: implications for the pathogenesis and treatment of Parkinson's disease. *Biochemistry* 40, 7812–7819(2001).
 19. Lee, H.J., Choi, C. & Lee, S.J. Membrane-bound A β -Synuclein Has a High Aggregation Propensity and the Ability to Seed the Aggregation of the Cytosolic Form. *Journal of Biological Chemistry* 277, 671–678(2002).
 20. Jo, E. et al. A β -Synuclein Membrane Interactions and Lipid Specificity. *Journal of Biological Chemistry* 275, 34328–34334(2000).

21. Valincius, G. et al. Soluble amyloid β oligomers affect dielectric membrane properties by bilayer insertion and domain formation: Implications for cell toxicity. *Biophysical Journal* 94, 2008.
22. Sparr, E. et al. Islet amyloid polypeptide-induced membrane leakage involves uptake of lipids by forming amyloid fibers. *FEBS Letters* 577, 117–120(2004).
23. Canale, C. et al. Natively Folded HypF-N and Its Early Amyloid Aggregates Interact with Phospholipid Monolayers and Destabilize Supported Phospholipid Bilayers. *Biophysical Journal* 91, 4575(2006).
24. Zhu, M. & Fink, A.L. Lipid Binding Inhibits α -Synuclein Fibril Formation. *Journal of Biological Chemistry* 278, 16873–16877(2003).
25. Hartley, D.M. et al. Protofibrillar Intermediates of Amyloid β -Protein Induce Acute Electrophysiological Changes and Progressive Neurotoxicity in Cortical Neurons. *Journal of Neuroscience* 19, 8876(1999).
26. Come, J.H., Fraser, P.E. & Lansbury Jr, P.T. A Kinetic Model for Amyloid Formation in the Prion Diseases: Importance of Seeding. *Proceedings of the National Academy of Sciences of the United States of America* 90, 5959–5963(1993).
27. Cannon, M.J. et al. Kinetic analysis of beta-amyloid fibril elongation. *Analytical Biochemistry* 328, 67–75(2004).
28. Xue, W., Homans, S.W. & Radford, S.E. Systematic analysis of nucleation-dependent polymerization reveals new insights into the mechanism of amyloid self-assembly. *Proceedings of the National Academy of Sciences* 105, 8926–8931(2008).
29. Collins, S.R. et al. Mechanism of prion propagation: amyloid growth occurs by monomer addition. *PLoS Biol* 2, e321(2004).
30. Sharp, J.S., Forrest, J.A. & Jones, R.A.L. Surface denaturation and amyloid fibril formation of insulin at model lipid-water interfaces. *Biochemistry* 41, 15810–15819(2002).
31. Urbanc, B. et al. Molecular Dynamics Simulation of Amyloid β Dimer Formation. *Biophysical Journal* 87, 2310–2321(2004).
32. Auer, S., Dobson, C.M. & Vendruscolo, M. Characterization of the nucleation barriers for protein aggregation and amyloid formation. *HFSP Journal* 1, 137–146(2007).
33. Wu, C., Lei, H. & Duan, Y. The Role of Phe in the Formation of Well-Ordered Oligomers of Amyloidogenic Hexapeptide (NF₃GAIL) Observed in Molecular Dynamics Simulations with Explicit Solvent. *Biophysical Journal* 88, 2897–2906(2005).
34. Gsponer, J., Haberthur, U. & Caflisch, A. The role of side-chain interactions in the early steps of aggregation: Molecular dynamics simulations of an amyloid-forming peptide from the yeast prion Sup35. *Proceedings of the National Academy of Sciences* 100, 5154(2003).
35. Nguyen, H.D. & Hall, C.K. Molecular dynamics simulations of spontaneous fibril formation by random-coil peptides. *Proc Natl Acad Sci US A* 101, 16180–16185(2004).
36. Jang, H., Zheng, J. & Nussinov, R. Models of β -Amyloid Ion Channels in the Membrane Suggest That Channel Formation in the Bilayer Is a Dynamic Process. *Biophysical Journal* 93, 1938(2007).
37. Crowet, J.M. et al. In Silico tilted properties of the 67–78 fragment of α -synuclein are responsible for membrane destabilization and neurotoxicity. *Proteins* 68, 936–947(2007).
38. Knecht, V. β -Hairpin Folding by a Model Amyloid Peptide in Solution and at an Interface. *The Journal of Physical Chemistry. B* (2008).doi:10.1021/jp8026513

39. Miao, M. et al. Sequence and Structure Determinants for the Self-aggregation of Recombinant Polypeptides Modeled after Human Elastin*. *Journal of Biological Chemistry* 278, 48553–48562(2003).
40. Kenney, J.M. et al. Amyloidogenic nature of spider silk. *FEBS Journal* 269, 4159–4163(2002).
41. Rauscher, S. et al. Proline and glycine control protein self-organization into elastomeric or amyloid fibrils. *Structure* 14, 1667–1676(2006).
42. Lindahl, E., Hess, B. & van der Spoel, D. GROMACS 3.0: a package for molecular simulation and trajectory analysis. *Journal of Molecular Modeling* 7, 306–317(2001).
43. Berendsen, H.J.C., van der Spoel, D. & van Drunen, R. GROMACS: A message-passing parallel molecular dynamics implementation. *Computer Physics Communications* 91, 43–56(1995).
44. Jorgensen, W.L., Maxwell, D.S. & Tirado-Rives, J. Development and Testing of the OPLS All-Atom Force Field on Conformational Energetics and Properties of Organic Liquids. *Journal of the American Chemical Society* 118, 11225–11236(1996).
45. Jorgensen, W.L. et al. Comparison of simple potential functions for simulating liquid water. *The Journal of Chemical Physics* 79, 926(1983).
46. Essmann, U. & others A smooth particle mesh Ewald method. *The Journal of Chemical Physics* 103, 8577(1995).
47. Berendsen, H.J.C. et al. Molecular dynamics with coupling to an external bath. *The Journal of Chemical Physics* 81, 3684(1984).
48. Hess, B. et al. LINCS: A linear constraint solver for molecular simulations. *Journal of Computational Chemistry* 18, 1463–1472(1997).
49. Miyamoto, S. & Kollman, P.A. Settle: An analytical version of the SHAKE and RATTLE algorithm for rigid water models. *Journal of Computational Chemistry* 13, 952–962(1992).
50. Pandit, S.A., Bostick, D. & Berkowitz, M.L. An algorithm to describe molecular scale rugged surfaces and its application to the study of a water/lipid bilayer interface. *The Journal of Chemical Physics* 119, 2199(2003).
51. Kabsch, W. & Sander, C. Dictionary of protein secondary structure: pattern recognition of hydrogen-bonded and geometrical features. *Biopolymers* 22, 2577–2637(1983).
52. Pettersen, E.F. et al. UCSF Chimera—A visualization system for exploratory research and analysis. *Journal of Computational Chemistry* 25, 1605–1612(2004).
53. Allen, M.P. & Tildesley, D.J. Computer Simulation of Liquids. (Clarendon Press: 1987).
54. Lee, J. et al. Instantaneous Amyloid Fibril Formation of \${\alpha}\$-Synuclein from the Oligomeric Granular Structures in the Presence of Hexane. *Biophysical Journal* (2008).

Table 1. List of simulations of GV4

System	Time (per run)	Peptides	Water molecules	Octane molecules	Box size (nm)	Number of runs	Total peptides	Time (total)	Concentration (water)	Concentration (slab) [†]
A	55.8 ns	2	1353! [!]	75	3.59x3.59x5.5	8	16	446 ns	0.027 M	0.082 M
B1	10 ns	8	15948! [!]	599	9.13x9.13x7.67	43	344	430 ns	0.042 M	0.090 M
B2	20 ns	8	5739! [!]	599	9.27x9.27x4.06	43	344	860 ns	—	0.090 M
C1*	50 ns	40	7960	1000	8.30x8.30x8	1	40	82 ns	—	0.439 M
C2	136 ns	40	7960	1000	"	1	40	219 ns	—	0.439 M
D	20 ns	8	12643!**	0	9.13x9.13x4.81	5	40	100 ns	0.042 M	—

*Run C1 was generated by addition of 8 chains for 10 ns, then 16 for 10 ns, then another 16 for another 12 ns (until all peptides were on the slab).

†Concentration on the slab is calculated assuming that the Z dimension of the interface is about 1 nm—this is the general size of the range of Z values for the center of mass of adsorbed chains.

! varies depending on conformation of peptide and the amount of space it takes up

** Number is slightly smaller than B1 because of removal of overlapping waters between top and bottom halves of box.

List of Figures

Figure 1: Sample conformations of GV4 separated into three categories based on their end-to-end distance. Hairpin and hairpin-like conformations are shown in the left panel; turns and turn-like conformations are in the center panel; and the right panel contains extended conformations.

Figure 13. Snapshots of Simulation C after 219 ns of simulation time. The top side of the slab (left) shows more ordered β -structures than the right side. Both sides show extended dimers, trimers, or other larger structures. The peptides are shown with valines in pink, glycines in a different color depending on the chain. The octane slab is shown in white.

Figure 14. Timescale of aggregation for one run from Simulation B2. a) 12 ns. b) 14 ns. c) 20 ns. d) 26 ns. Valines are colored in pink, glycines are colored using a different color for each chain. The slab is shown in white.

Figure 16. Endpoints of runs from simulation D. Each box represents the clusters of peptides found after the end of 20 ns of simulation time for a different replicate of D.

Figure 15. One run in Simulation D, after 160 ns of additional simulation time, showing a large globular aggregate. Color is similar to that in Figure 14.

Figure 1: Simulation snapshots showing adsorption of one chain to the octane surface. a) Adsorption is initiated by interaction between at least one valine side chain (shown in pink) and the octane slab (shown in blue) at 1.5 ns. b) After 6 ns, the peptide is lying flat on the slab, and has taken on an extended conformation.

Figure 2: Proportion of GV4 chains remaining fully solvated over the timescourse of Simulation B1. Fitted with an exponential fit.

Figure 3: Densities and distributions of various atoms with the interface. a) Density profile for Simulation C2 showing distribution of backbone, $C\alpha$, and Val $C\gamma$ atoms. b) Axial distribution of valine $C\gamma$ atoms and $C\alpha$ atoms normalized with respect to the slab surface.

Figure 4: The number of waters in the first hydration shell of the $C\gamma$ atoms compared to the number of backbone bound waters. a) Simulation A; b) Simulation D; c) Simulation B1; d) Simulation B2; e) Simulation C1; f) Simulation C2. A progressive increase in dehydration is seen in panels (c) through (f).

Part C: End-to-end distance effects of slab binding

Figure 5: Normalized distribution of d_{ete} . Simulations on the slab are listed at the top, in order of increasing timescale and concentration. Simulations in water are shown at the bottom. Y axis is

arbitrary. For simulations on the slab, the plateau (> 2 nm) grows and the hairpin conformation (centered at ~ 0.66 nm) becomes less prevalent over time, both effects not observed in water. Standard error is depicted as shading around the lines.

Figure 6: Time-evolution of d_{ete} for simulations B1 and B2. Note that most of the extension occurs in the first 10 ns, the bulk of the exchange appears between the intermediate ($0.66 - 1.30$ nm) and extended conformations (> 1.30 nm). There is a marked exchange between the intermediate and extended conformations.

Figure 7: Ratios of closed, intermediate and extended conformers in simulations. Systems in a) are on the slab, systems in b) are in water. Simulation A is included as a control in (b) for comparison.

Part D: Hydrogen bonding

Figure 8: Hydrogen bond time evolution. a) Simulation B1 and B2. Note the linear increase for the first 6 ns, followed by an increase at a slower rate. b) Simulation C1 and C2. At high concentration and longer time-scales the number of intermolecular hydrogen bonds formed between the chains keeps increasing gradually after an initial surge of formation of new bonds and is far greater than that of the intramolecular bonds, which maintain a baseline level of ~ 0.5 bonds / chain. c) Simulation D. A very rapid initial increase in intermolecular hydrogen bonds is apparent, which tapers off after the initial aggregation occurs.

Figure 9: d_{ete} distribution, separated by type of hydrogen bonding. a) Simulation B2: There is a slight plateau at $d_{ete} > 2$ nm for peptides with only intermolecular bonds, compared to those with no hydrogen bonds. The peptides with both inter-peptide and intra-peptide hydrogen bonds or intramolecular bonds only remain in more closed conformations in comparison to all other peptide chains. b) Simulation C2. Over a longer time-scale at high concentrations, there is a separation between the distance distributions of peptides without any hydrogen bonds and those with only intermolecular bonds. The plateau at 2 nm or greater is larger in size than for Simulation B2. c) Simulation D. The overall separation is similar to that with the slab systems. However, more of the peptides that have either intermolecular hydrogen bonds or have no hydrogen bonds are in the lower range of the distance spectrum. Standard error is represented by the shaded regions around the lines.

Part E: Aggregates

Figure 10: Timescale of aggregation. a) Aggregation for Simulations B1 and B2. b) Aggregation for Simulation C1 and C2.

Figure 11. Hydrogen bonding, separated by type and number of hydrogen bonds, compared to backbone bound waters.

Part F: Secondary Structure

Figure 12: Secondary structure time evolution of GV4 systems. a) B1 and B2. b) C1 and C2. The beta sheets increase linearly for the first 5-6 ns, after which they begin increasing in a slower rate.

Figure 1

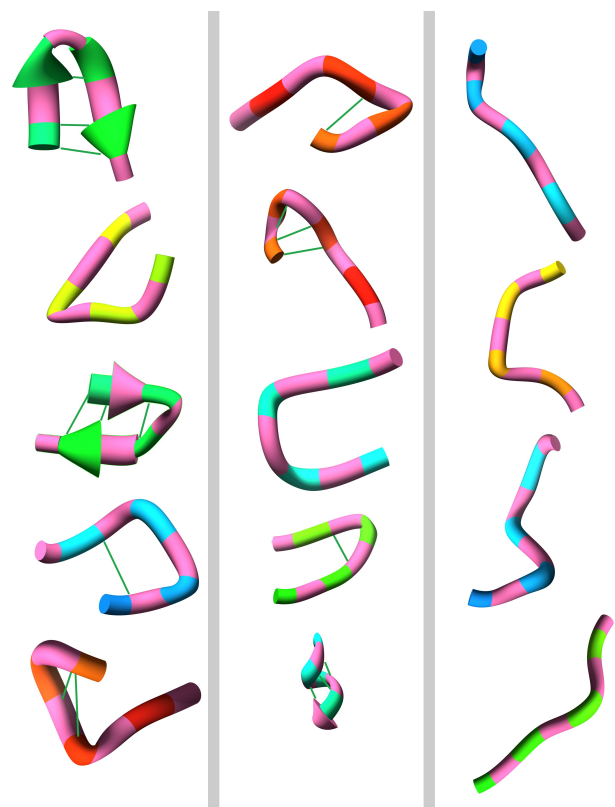


Figure 13

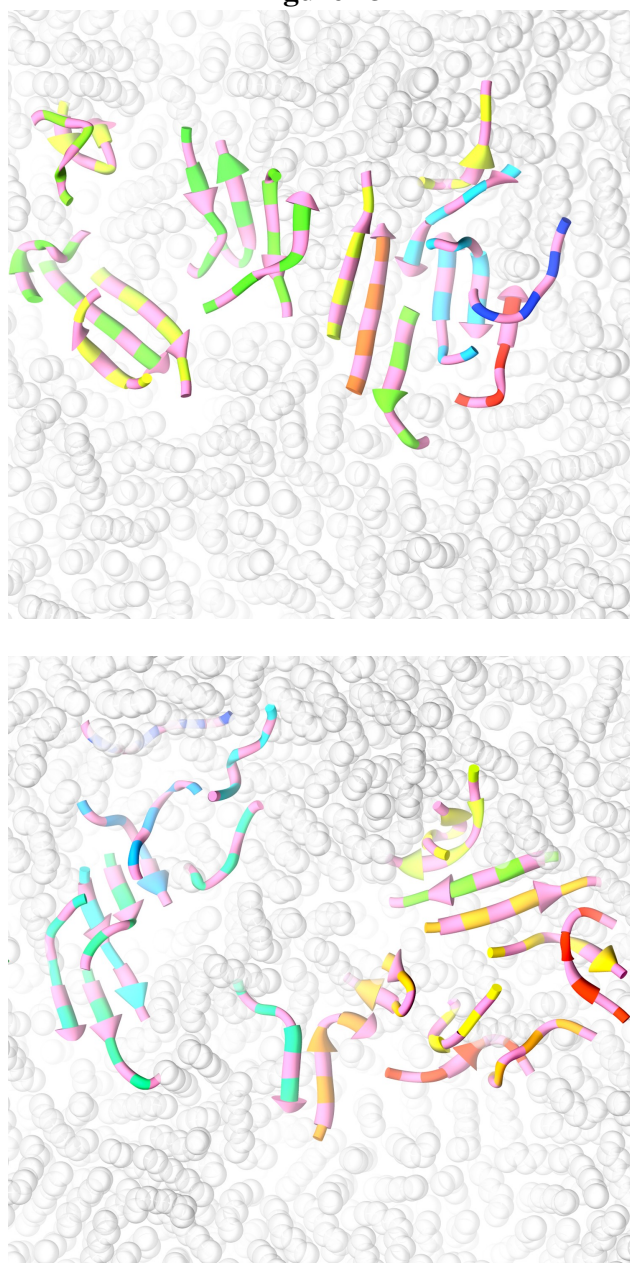


Figure 14

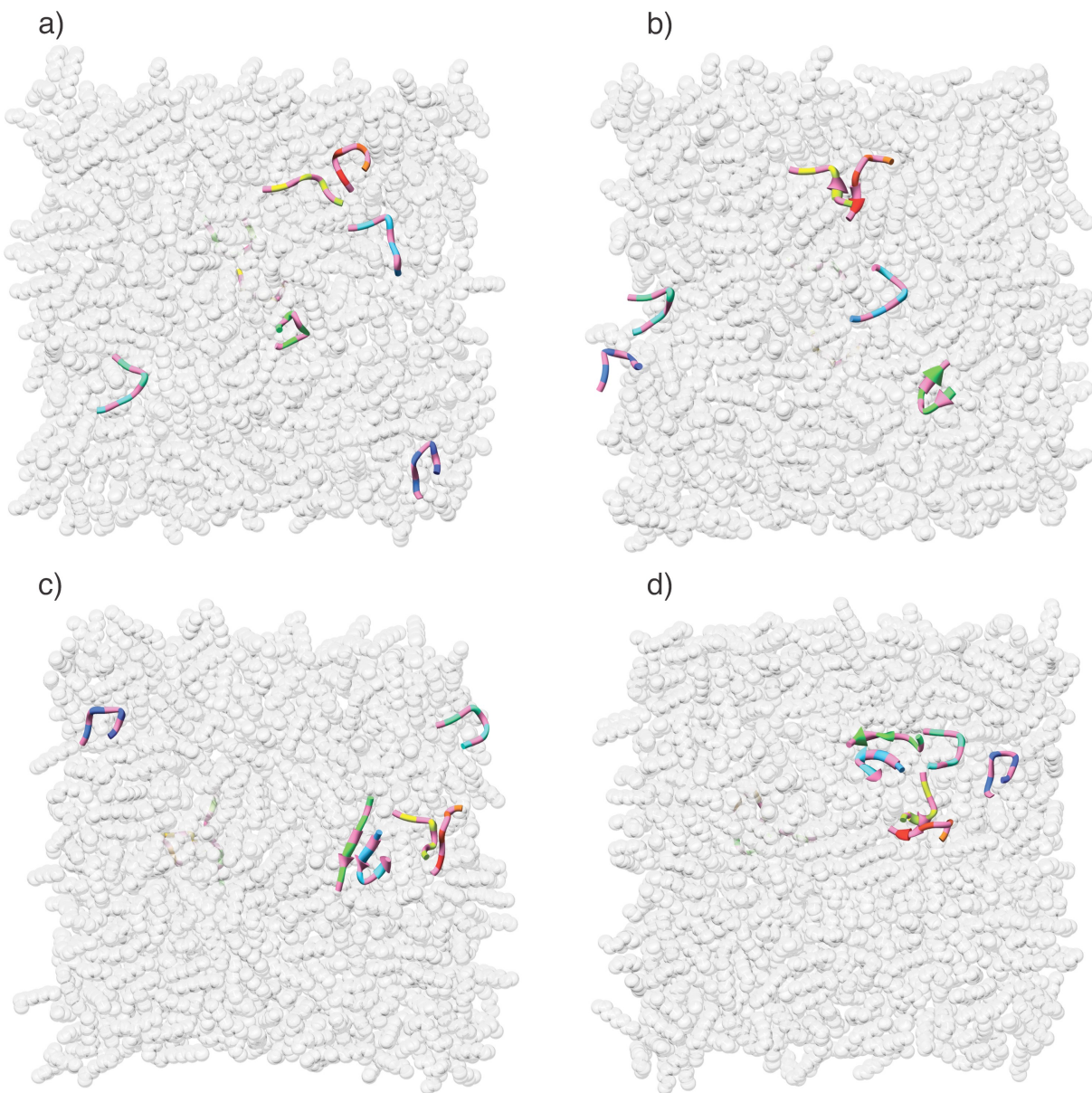


Figure 16

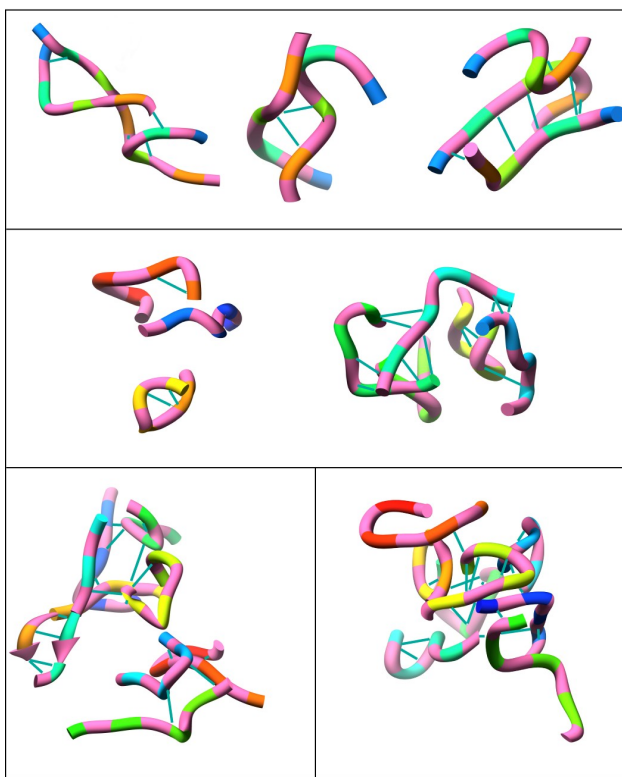


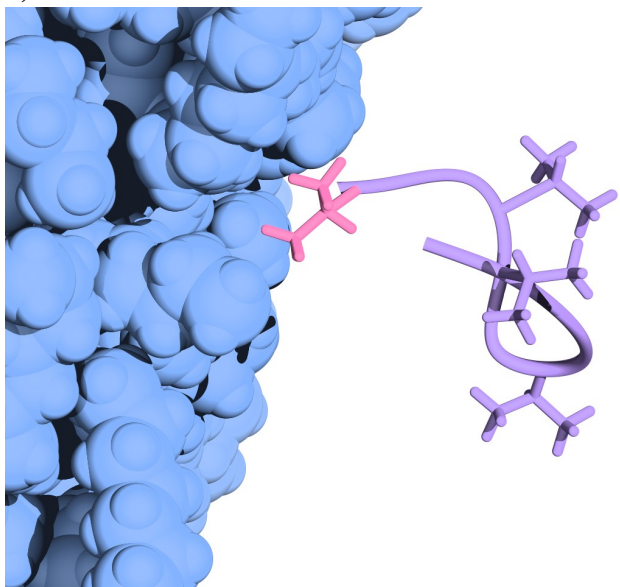
Figure 15



**** redo with HB ****

Figure 1

a) 1.5 ns



b) 6.5 ns

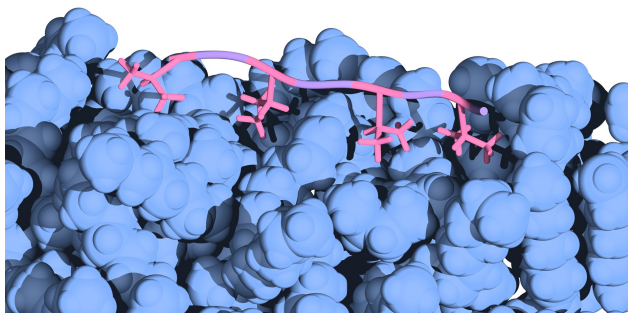


Figure 2

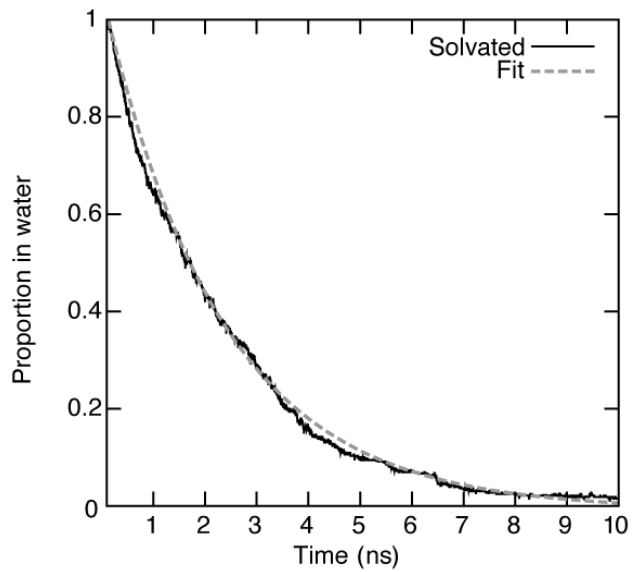
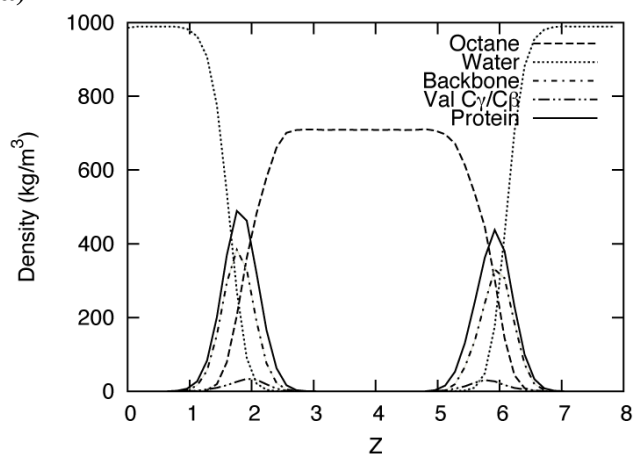


Figure 3

a)



b)

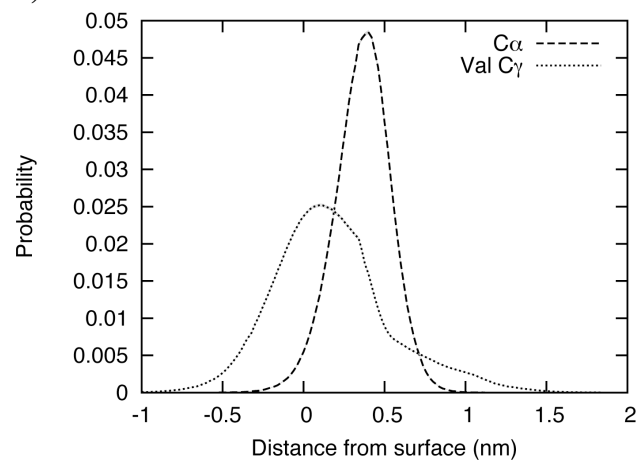


Figure 4

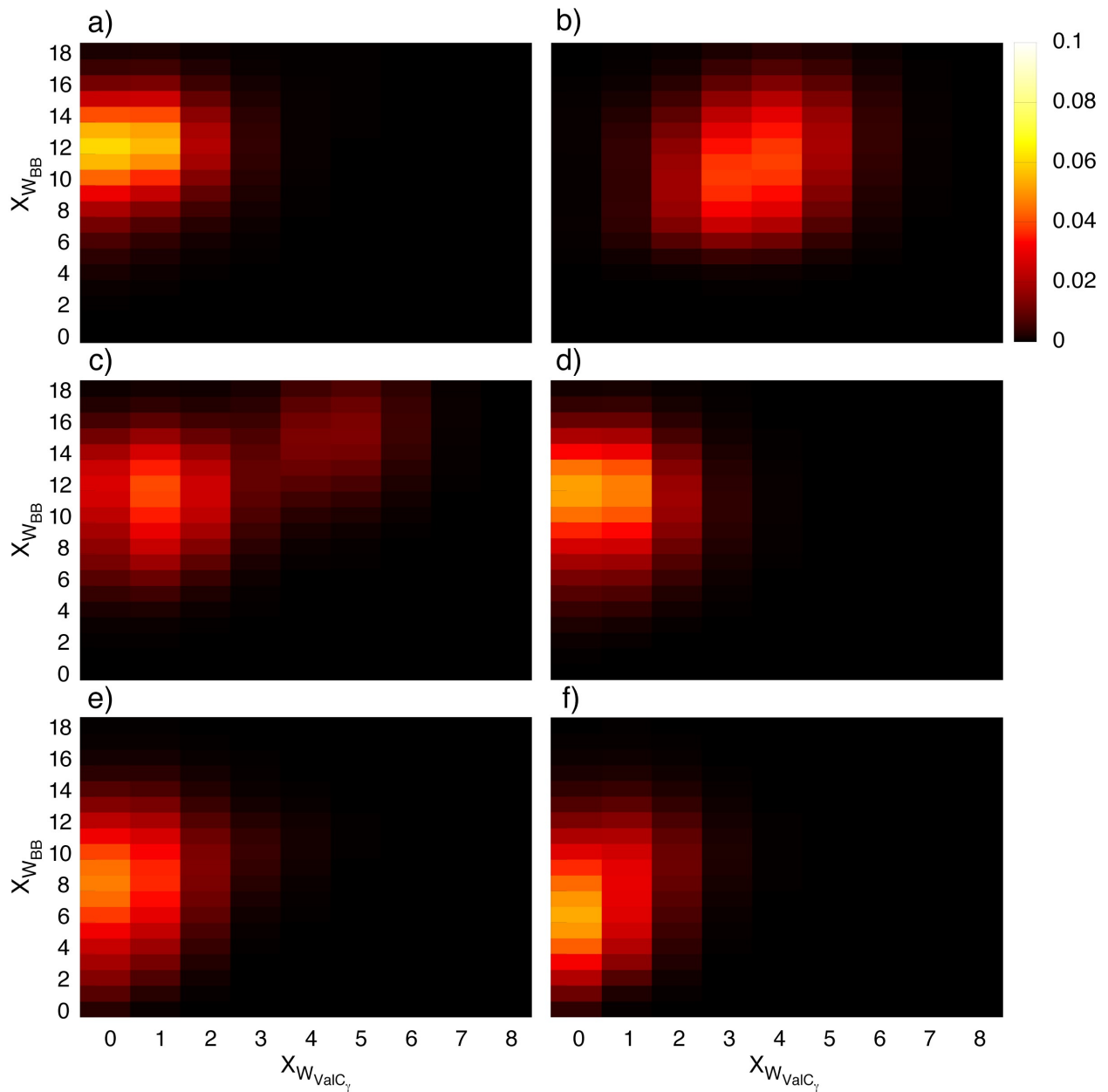


Figure 5

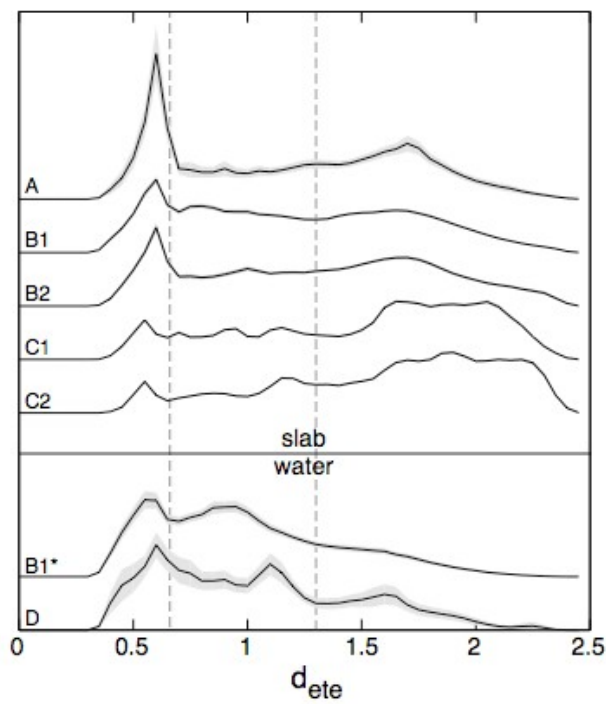


Figure 6

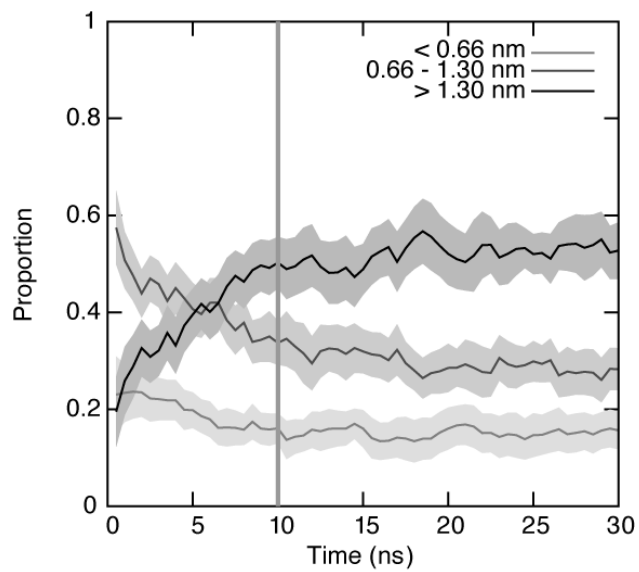
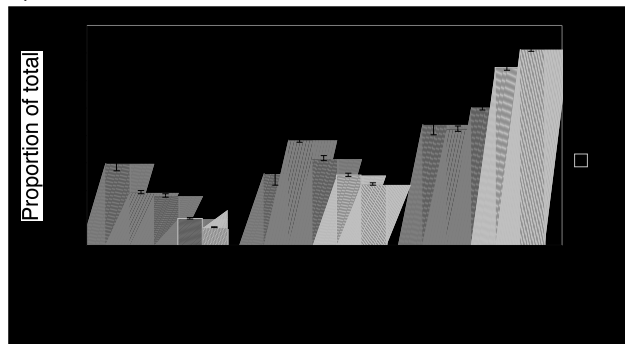


Figure 7

a)



b)

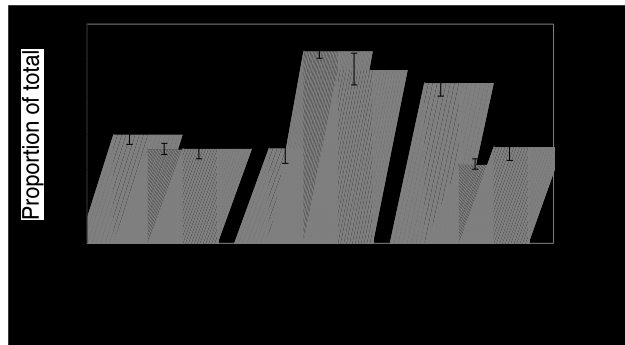


Figure 8

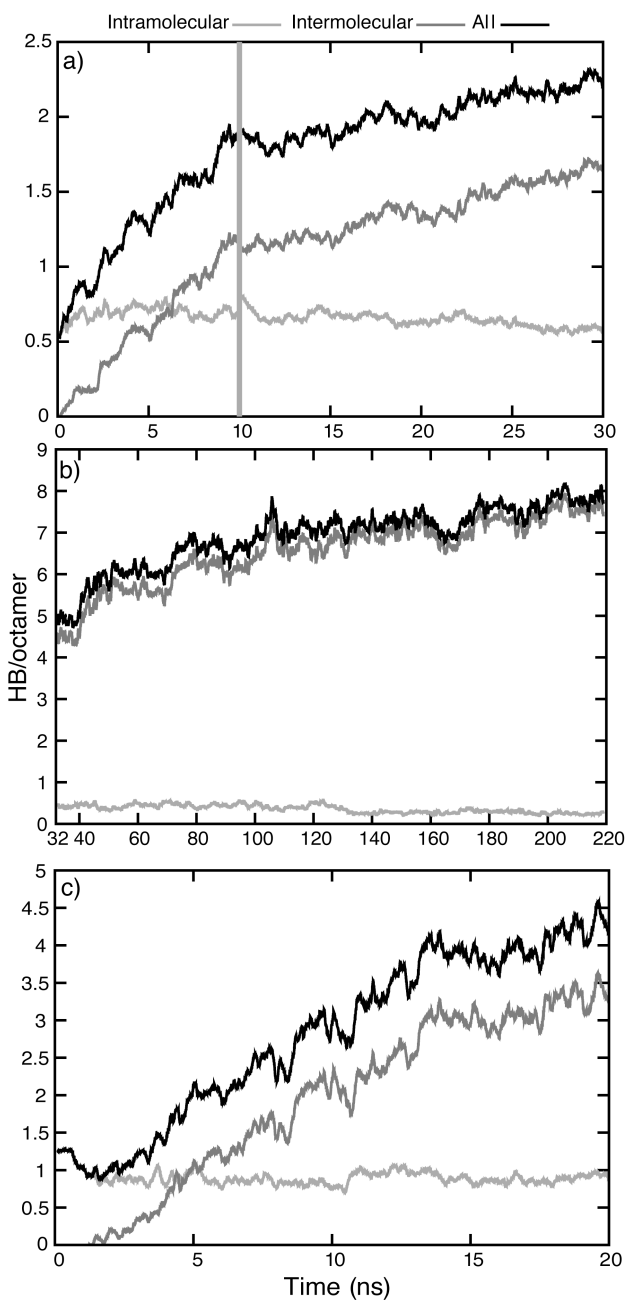


Figure 9

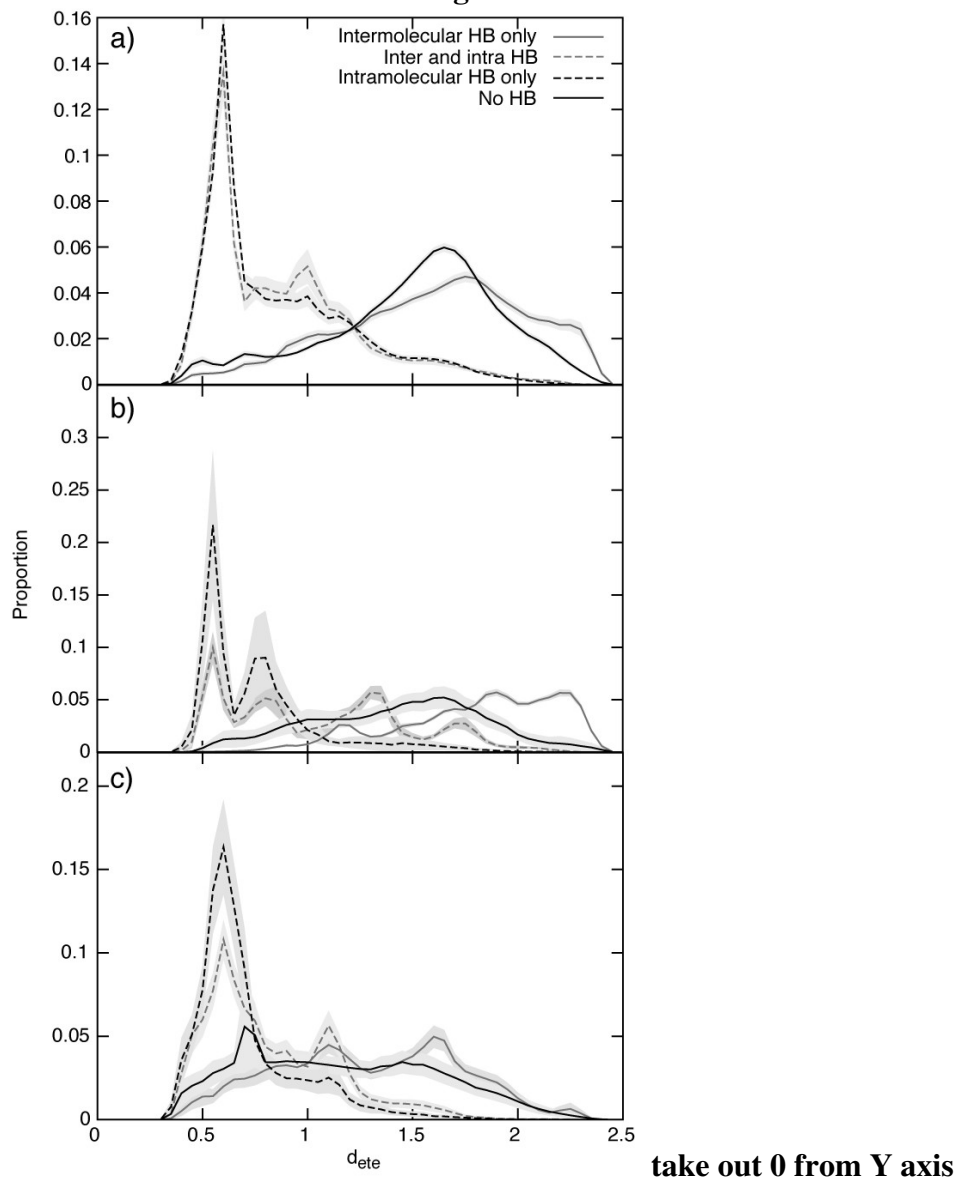


Figure 10

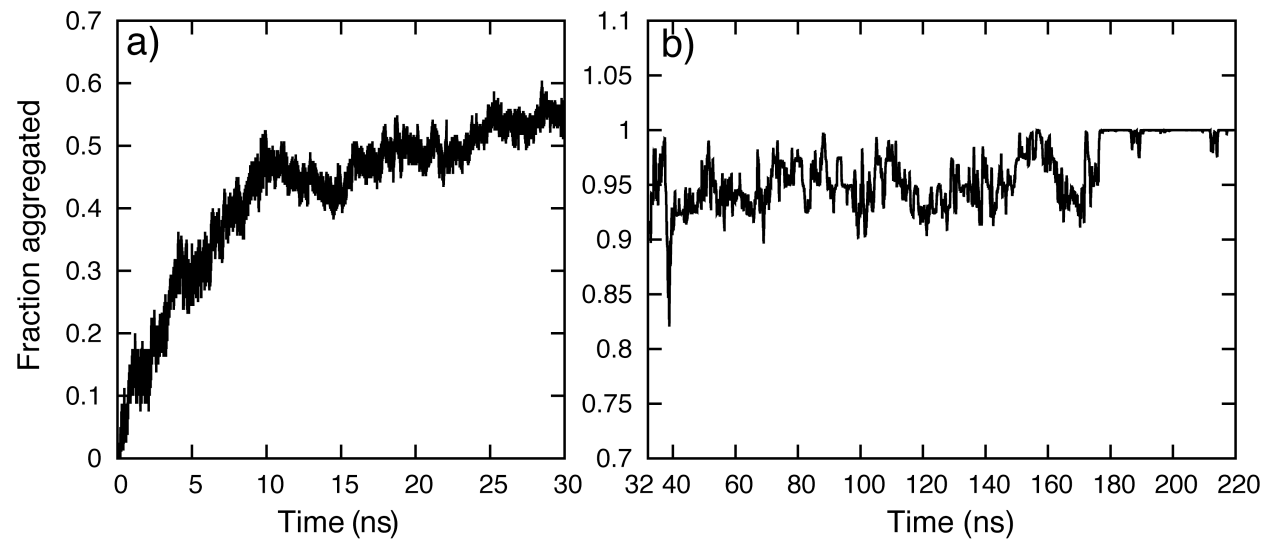
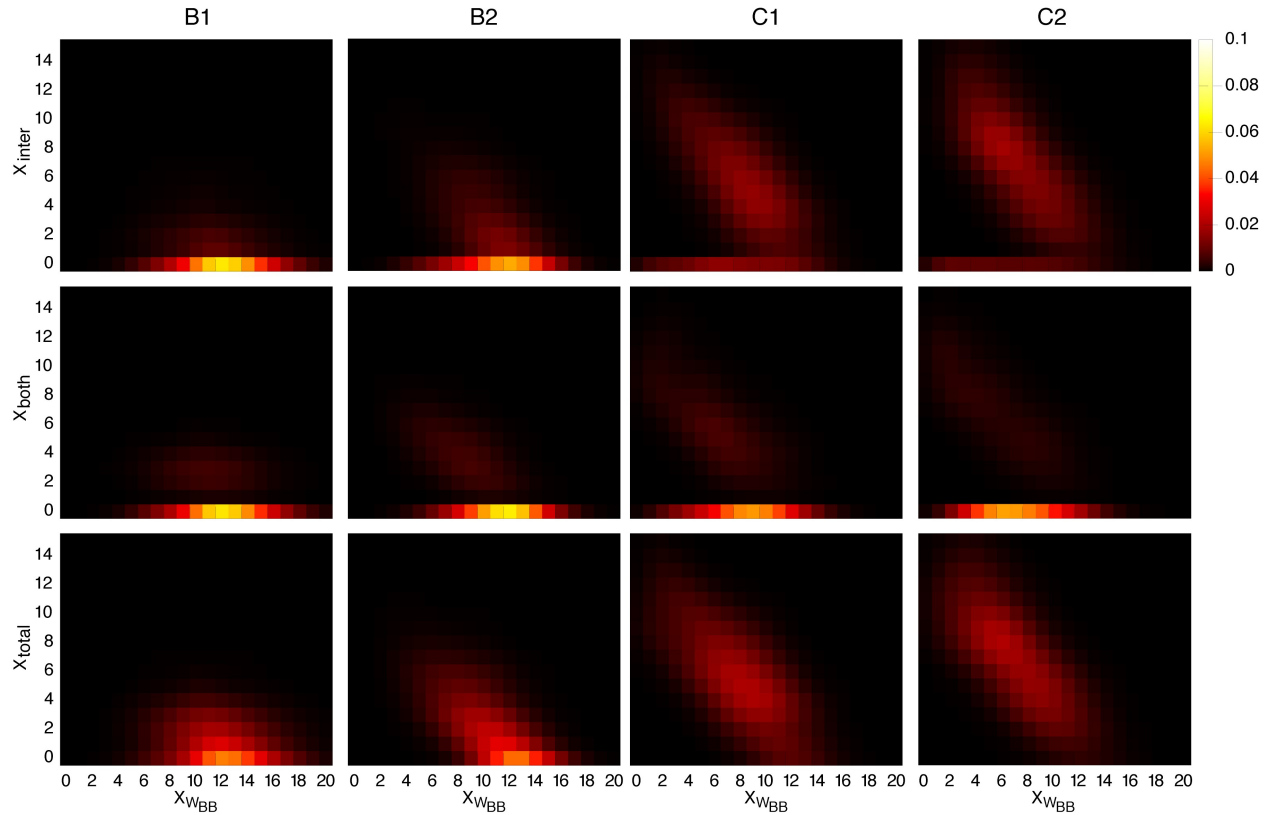
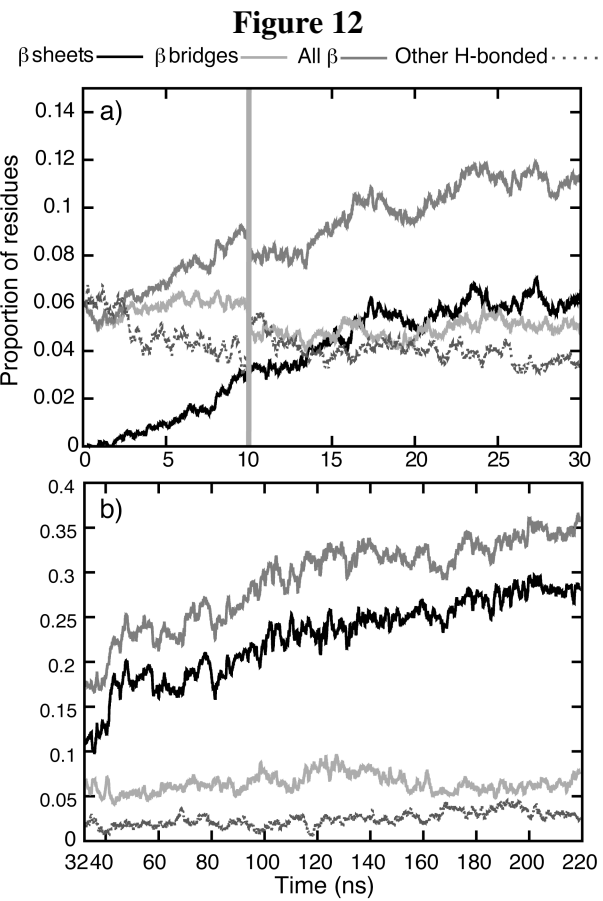


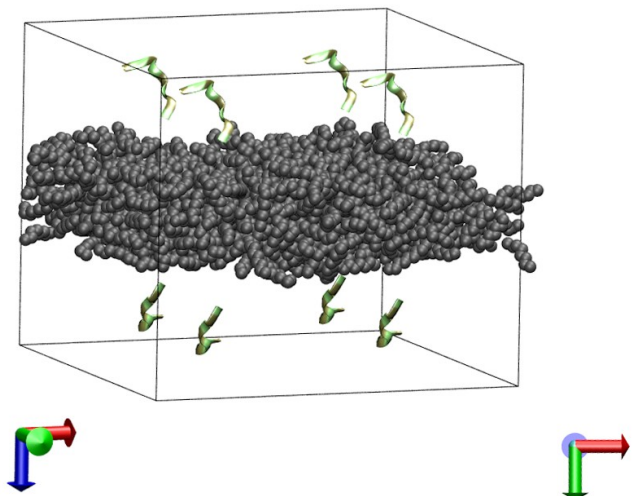
Figure 11





Supplementary Figure 1. representative starting structure (for Simulation B1) [supplementary]

Side view



Top view

